Retro-fit Solutions for Energy Efficient Shipping

Ship Science Report n^{o}148

Faculty of Engineering and the Environment

Ship Science

R.E. Collison, M.C. James, S.R.Turnock, D.A. Hudson

January 2013

UNIVERSITY OF Southampton

Abstract

With the increase in fuel prices and growing pressure on the marine industry to reduce greenhouse gas emissions, there is a demand for both new and current ships in operation to develop novel ways to reduce their fuel consumption. In January 2013, the International Maritime Organisation (IMO) provided mandatory methods on how both new and existing ships will be assessed on their emissions via the Energy Efficiency Design Index (EEDI) and the Ship Energy Efficiency Management Plan (SEEMP) respectively. Existing ships are less suitable for major design changes, so they must rely on engine room systems upgrades or the use of retro-fit devices.

This research paper presents how the efficiency of an existing tanker hull form could be increased by 10% with the use of cost-effective retro-fit solutions. A method, involving CFD simulations performed using OpenFOAM® and validated with wind tunnel tests, is explained. An in-house code, based on the Blade-Element Momentum Theory (BEMT), is used to provide some propeller characteristics: efficiency, torque and thrust coefficients. Although, the efficiency output from the BEMT code is not the propulsive coefficient, η_D, the different appendage configurations may still be directly compared using this efficiency, denoted η_{BEMT} throughout this paper. This procedure successfully detects changes in propeller efficiency at model scale due to devices and thus provides a route to investigate a wide variety of devices. Preliminary results highlightes that efficiency gains up to 3% could be obtained with vanes and up to 9% with flow increasing ducts.

Acknowledgements

We would like to acknowledge the following people:

The project supervisors, Professor Stephen Turnock and Dr Dominic Hudson, for their continued help and advice during the year.

The project sponsors without whom this project would not have been possible.

All the Ship Science and Faculty staff and research fellows for their support and time for consultation and advice.

Contents

List of Figures

List of Tables

1 INTRODUCTION

1.1 Background

With the increase in fuel prices and growing pressure on the marine industry to reduce greenhouse gas emissions, there is a demand for both new and current ships in operation to develop novel ways to reduce their fuel consumption. In January 2013, the International Maritime Organisation (IMO) provided mandatory methods on how both new and existing ships will be assessed on their emissions via the Energy Efficiency Design Index (EEDI) and the Ship Energy Efficiency Management Plan (SEEMP) respectively. Existing ships are less suitable for major design changes, so they must rely on engine room systems upgrades or the use of retro-fit devices.

1.2 Aims and Objectives

The aim of this project is to improve the efficiency of a specific vessel by 10% in order to meet the Ship Energy Efficiency Management Plan devised by the IMO. This improvement should be made with the use of cost-effective retro-fit solutions.

To achieve this aim, a set of objectives was established:

- Produce a 3D model and obtain a linesplan of the vessel from available offset data;
- Carry out an initial stern flow investigation in the wind tunnel using a geosim ship model (naked hull);
- Perform a Computational Fluid Dynamics (CFD) simulation representing the initial wind tunnel test;
- Validate the CFD based on the wind tunnel test results and investigate potential retro-fit devices using CFD;

1.3 Literature Review

1.3.1 IMO Regulations

By 2020, the International Maritime Organisation (IMO) aims at reducing CO_2 emitted per tonne of cargo transported per kilometer (tonne/km) by 15% to 20%. In order to achieve this, the IMO has devised new mandatory regulations in January 2013. Indeed,

the Energy Efficiency Design Index (EEDI) is now applicable to all new ships. This index assesses the ratio of emissions over the benefit to the society.

For the IMO to accomplish its aim of reducing greenhouse gas emmisions by 2020, it was necessary to put in place regulations concerning exiting ships. This is covered by the Ship Energy Efficiency Management Plan (SEEMP). The SEEMP provides guidance to owners of both new and existing ships on how to monitor their ships and fleet efficiency performance over time in a cost effective manner. The Energy Efficiency Operational Indicator (EEOI) is used in the SEEMP plan as a benchmark. The EEOI gives ships operators a measure of their fuel efficiency. This indicator may be expressed conceptually as:

$$EEOI = \frac{\text{Fuel x } CO_2 \text{ conversion factor}}{\text{Cargo quantity x Distance}} \tag{1.1}$$

Thus, the EEOI takes into account several voyage data such as fuel consumption, voyage distance and cargo quantity (tonnes, TEU, persons,etc.).

Figure 1 shows IMO suggested technologies to be in agreement with the new regulations (EEDI and SEEMP). In this report, retro-fit devices will be considered as a mean of applying the SEEMP for existing ships in a cost effective manner. The various types of retro-fit devices are described in the section below (1.3.2).

	EEDI reduction measure	SEEMP Related measure
1	Optimised hull dimensions and form	Engine tuning and monitoring
2	Lightweight construction	Hull condition
3	Hull coating	Propeller condition
4	Hull air lubrication system	Reduced auxiliary power
5	Optimisation of propeller-hull interface and flow devices	Speed reduction (operation)
6	Contra-rotating propeller	Trim/draft
7	Engine efficiency improvement	Voyage execution
8	Waste heat recovery	Weather routing
9	Gas fuelled (LNG)	Advanced hull coating
10	Hybrid electric power and propulsion concepts	Propeller upgrade and aft body flow devices
11	Reducing on-board power demand (auxiliary system and hotel loads).	
12	Variable speed drive for pumps, fans, etc.	
13	Wind power (sail, wind engine, etc.)	
14	Solar power	
15	Design speed reduction (new builds)	

Figure 1: Technologies for EEDI reductions and SEEMP related measures (Bazari *et al.* 2011)

1.3.2 Current retro-fit technology

Energy efficiency devices rely on two main ways to improve the efficiency of the ship: devices that increase the propulsive efficiency of the ship and those that supplement the power requirement of the ship by harnessing renewable sources. The latter include systems such as kite power, solid sails and Flettner rotors (Jijun *et al.* 2011 and Craft *et al.*), along with solar power supplementation. Systems of this nature generally require large general arrangement and structural alterations. The propulsive efficiency of the ship should therefore be analysed, since the retro-fit devices in this area are generally less intrusive to the ship, and thus potentially more economically viable.

The propulsive efficiency of a ship is characterised by the Quasi-Propulsive Coefficient (QPC), which is a function of the open water, hull and relative rotative efficiencies (Molland *et al.* 2011). Of these components, the open water efficiency provides the greatest opportunity for improvement as the other two are close to unity (in the order of 0.9). The open water efficiency can be described as the product of the ideal efficiency (based on axial momentum theory, allowing a finite number of blades), losses due to fluid rotation induced by the propulsor and losses due to blade friction (Molland *et al.* 2011). A breakdown of this efficiency component into its relative parts revealed areas where improvements could be made. Losses in efficiency due to blade friction could be improved with blade coatings or even propeller cleaning. It is possible to reduce losses due to fluid rotation by minimising the relative rotation of the fluid in the downstream transverse planes, pre- and post-swirl devices may improve this.

Energy saving devices (ESD's) usually work around one of two principles to increase the open water efficiency; increasing the speed of flow through, or changing the direction of flow entering and leaving the propulsor.

Increasing the speed of flow through the propeller can be achieved using a wake equalising duct (WED). This type of duct usually has a foil cross section and the diameter of the leading edge is less that that of the trailing edge, forcing the fluid through the duct and therefore accelerating the flow. The effects of wake equalising ducts have been studied by the likes of Dang *et al.* (2011) and Mewis *et al.* (2011). The Mewis duct is a combination of a WED and a pre-swirl stator with the supporting fins of the WED inducing swirl into the flow entering the propeller (Mewis *et al.* 2011). Vortex generators are devices located upstream on the propeller. They work by inducing a vortex into the

flow, which builds down the length of the ship until it reaches the propeller. The vortex tends to follow the side of the ship, thus reducing any areas of decelerating flow before the propeller plane.

Pre- and post-swirl devices act to induce a tangential velocity into the flow around the propeller plane. This additional flow component acts to cancel out the tangential flow induced by the propeller, thus maximising the proportion of axial flow in the wake (Zondervan *et al.* 2011). The addition of pre- and post-swirl devices helps to reduce the losses in propeller efficiency, due to propeller induced fluid rotation (Molland *et al.* 2011). Additional resistance from the rudder due to tangential flow from the propeller can be countered using post-swirl devices. Hub vortices produced by the propeller may increase the rudder's resistance, as well as reducing its effectiveness and cause cavitation on its surface. This can be reduced by means of a Costa bulb (Collazo *et al.* 2010) or devices working on similar principles such as the Rolls Royce PROMAS System. Additionally, propeller boss cap fins could be used to reduce propeller hub vortices; hence decreasing the shaft torque and increasing the thrust (Hansen *et al.* 2011).

There are many retrofit devices currently available, each claiming in the region of less than 10% efficiency gains. These figures are not always trustworthy as they were measured by the developer of the system and may therefore have been subjected to exaggeration. The data sets for each device may not have been obtained in a standard way. Indeed, a range of wind tunnel, towing tank and CFD testing was conducted for the devices, but none were subjected to all three. It may therefore have been difficult to make a comparison between devices. The magnitude of the efficiency gains due to a device is very dependent upon the ship type and propulsor operating conditions. As a result relative efficiency gains should be analysed for individual ships before deciding which device to choose.

There are many devices that are currently used on ships including: Mewis Ducts, PROMAS systems, swirl devices and WEDs. Vortex generators are usually a specific shaped plate, welded to the side of the ship upstream of the propeller.

1.3.3 Computational fluid dynamics

Computational Fluid Dynamics (CFD) is a tool to study the fluid flow characteristics around, within and between bodies. It attempts to solve the Navier-Stokes equations numerically, based on the equations of continuity, momentum and energy, governing the fluid flow.

The development of CFD was initiated by Richardson (1910) with the publication of a report on mathematical models using central differences to the Royal Society. Further developments were only made 50 years thereafter with the Marker and Cell computing method developed by Harlow and Welch in 1965. In the 1970s, finite difference methods were introduced to solve the Navier-Stokes equations. In the 1980s, with the creation of finite volume methods, CFD started to find commercial applications, especially in the aeronautic industry with Boeing (Forester 2005).

It is only in the 1990s that CFD found its application in the marine industry. This late start may be explained by the dominance of the viscous forces around ships hulls, increasing the complexity of the problem to be solved. To begin with, the flow around a hull was computed using surface panel methods. With the increase in computational power, numerical methods were then extended to solving the non-linear Navier-Stokes equations. The most accurate technique is Direct Numerical Simulation (DNS). This provides a solution for all flow features at all spatial and temporal scales. However, due to the high level of turbulence created, it is impractical to simulate typical engineering problems (Moin and Mahesh 1998). A more feasible method would be to use a Large Eddy Simulation (LES) as this eliminates the small scale turbulence effects within the flow using low-pass filtering. This technique was used to calculate the resistance of the Kriso tanker KVLCC2 (Kornev *et al.* 2010) for which the results were presented at the 2010 Gothenburg Workshop. LES showed that the resolution of the mesh in the near-wall region was too coarse to effectively evaluate the resistance. Fortunately, most engineering problems do not require the evaluation of every eddy. As a result, the concept of time-averaging may be implemented; this gives rise to the Reynolds Averaged Navier-Stokes (RANS) equations. The results obtained for the KVLCC2 and many other cases using a RANS-based approach, when compared with experimental data, confirmed the accuracy of using such a method. Therefore, complex problems may now be numerically modelled using incompressible RANS equations within a relatively short period of time.

With the advances in computational resources, the range of CFD applications in the marine industry has rapidly expanded. Several conferences and workshops organised by the Resistance Committee associated with the ITTC have supported this development. Research carried out over the past two decades covers: effects of wind drag on accommodation block (Nakashima *et al.* 2009), flow field and wave system around a ship (Souto-Iglesias *et al.* 2006), resistance and propulsion studies (Kornev *et al.* 2010), trim

optimisation study (Xing *et al.* 2008), added resistance (Orihara *et al.* 2003), etc. More recently, the use of energy saving devices has been actively studied (Hafermann *et al.* (2010), Makino *et al.* (2008), Maria *et al.* (2011), Carstens *et al.* (2009)), as shown in Figure 2. Extensive sets of experiments were performed in the above research to validate the CFD studies. Thanks to a reasonably good accuracy with experimental results, the efficiency of RANS-CFD allows time for ship design optimisation process to be performed before undertaking model testing. Furthermore, CFD appears to be an inexpensive design tool, when compared to the cost of running experimental tests. However, great care must be taken in assessing the level of uncertainties.

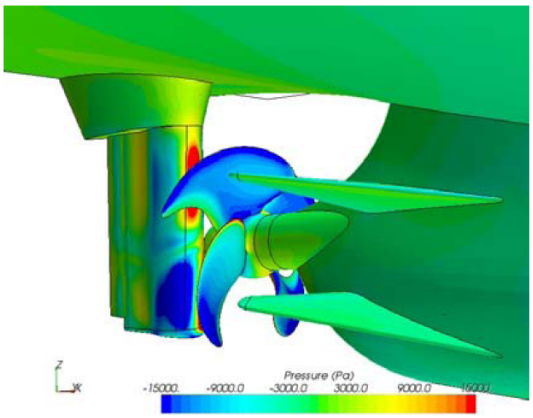

Figure 2: Pressure distribution on the suction side of the propeller with the use of fins (Carstens *et al.* 2009)

Multiple software packages are available to naval architects to conduct the various aspects involved in ship design. There are several commercial packages available; however, these are not tailored to the marine industry needs. In such applications, free-surface effects are almost always required but only a few commercial codes offer techniques, such as Volume of Fluid, that can take them into account. A company with a specific type of engineering problem may also choose to develop their own bespoke code. This option is not widely used due to the high level of expertise required. Alternatively, open source packages such as OpenFOAM may be used. Extensive validation through university research and companies (Cordier *et al.* 2011) revealed the increase in accuracy of such solvers. The fast development of OpenFOAM and the inexpensive computational resources promises a future for CFD open source codes.

1.4 Tanker Hull Form

The main particulars of the tanker hull form studied in this project are presented in Table 1. The reference system used throughout the study is presented in Figure 3.

Table 1: Ship particulars

Length, Over All	**(m)**	183.88
Length, Between Perpendiculars	**(m)**	174.00
Breadth	**(m)**	32.20
Depth	**(m)**	18.80
Draft, Summer Load	**(m)**	12.42
Deadweight, Summer Load	**(Tonnes)**	47084
Displacement, Summer Load	**(Tonnes)**	57054
Draft, Ballast	**(m)**	7.50
Displacement, Ballast	**(Tonnes)**	32563
C_B	-	0.7994
Service speed	**(Knots)**	15.5

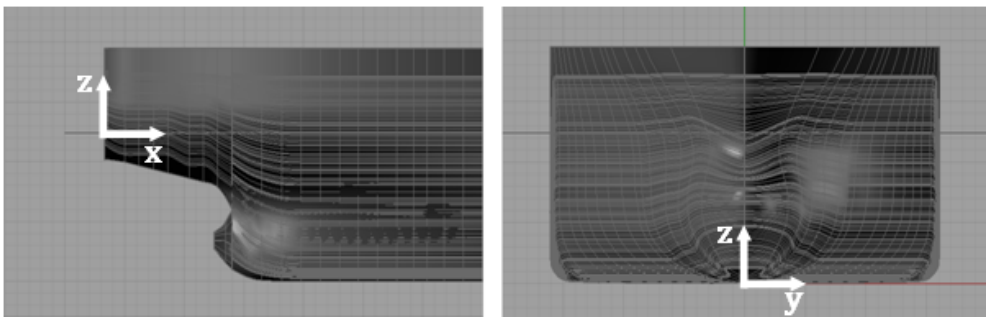

Figure 3: Reference system

1.5 Report Layout

First, background theory is introduced in Section 2. The experimental apparatus and methodology used for the wind tunnel test is described in Section 3, followed by the CFD simulations set-up in Section 4. Wake traverse and flow field simulation results for the naked hull are presented in Section 5, along with boundary layer and pressure field validations for the use of a truncated model in a wind tunnel. Investigations of possible retro-fit devices are found in Section 6. This is followed by Section 7 which presents

an initial set-up for a CFD simulation including a free-surface. A conclusion is offered in Section 8, and based on the findings of this preliminary investigation, possibilities for further research and improved experimental work on the use of retro-fit devices for energy-efficient shipping are discussed in Section 9.

2 BACKGROUND THEORY AND COMPUTATIONAL TOOLS

2.1 Ship Modelling

Based on available offsets, the tanker hull form was modelled in 3D using Rhinoceros and Grasshopper. Rhinoceros is a 3D design software package commonly used in ship design. It uses Non-Uniform Rational Bezier Splines (NURBS) to define curves and surfaces. Grasshopper is a plug-in for Rhinoceros, which allows the user to write a Rhinoceros script with a user-friendly interface. This script allows a semi-automatic design process, in the sense that the user only has to enter the points defining the different sections. This reduces human error when trying to adjust the hull shape.

NURBS curves are defined by a set of points called 'control points'; which, when linked together, form a 'control polygon'. The polygon encloses the NURBS curve; the smoothness of the curves may be controlled by applying a weight to the control points. Hence, although being fair, NURBS curves do not pass through the points originally defined. NURBS curves are useful to design new hull shapes with a set of fair lines. They are therefore difficult to use when reverse engineering.

Furthermore, a grasshopper script was created to develop a 2D linesplan from a 3D model, necessary for the wind tunnel model construction.

2.2 Blade-Element Momentum Theory

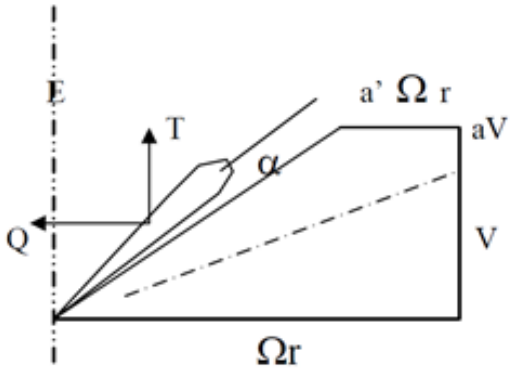

Figure 4: Blade element

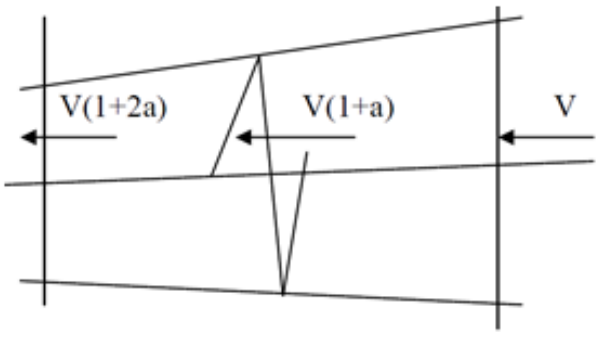

Figure 5: Momentum

The Blade Element Theory (BET) identifies the developed forces for a given flow incidence at a given section. The BET approach provides information on the action of the blade section, but not the momentum changes induced by the velocity factors a and a' (Molland *et al.* 2011). The momentum changes are therefore needed to calculate the forces applied on the blade section.

The coupling of both theories leads to the Blade-Element Momentum Theory (BEMT). The local forces obtained from the BET are matched with the momentum changes occurring in the fluid flowing through the propeller disc at different radii. The iterative process for the BEMT approach is presented in Figure 6.

This theory models the propeller as an actuator disc. In order to correct this unrealistic assumption, a correction factor (Goldstein, K) is introduced. However, other BEMT limitations cannot be eliminated. It cannot be applied to heavily loaded or highly skewed propellers and the effect of the tangential velocity is neglected. Furthermore, numerical errors are induced with the use of Simpson's rule to perform the integration across the different radii.

An in-house Fortran code, based on the BEMT process, was written by Professor Molland and Professor Turnock, at the University of Southampton. Doctor Alex Phillips, fellow researcher, implemented a Matlab code, 'Proplin3', in 2010. This code requires several input parameters: ship advance ratio, pitch ratio at 0.7 radius, BAR, number of blades and the wake matrix. The last parameter is created using the local non-dimensional ship axial velocity. The radial and circumferential locations correspond to the rows and columns respectively. This program provides the user with information regarding the propeller characteristics: efficiency, torque and thrust coefficients. The efficiency output from the BEMT code is not the propulsive coefficient, eta_D. It cannot be used for powering calculations, thus leading to the inability to derive an accurate cost analysis. This efficiency includes the open water efficiency, but only parts of the hull and relative rotative efficiency, since the thrust deduction factor is not considered in the BEMT code. However, the different appendage configurations can still be directly compared using this efficiency denoted η_{BEMT} throughout the report. This method can thus be used to compare all results obtained from wind tunnel tests, towing tank tests and CFD.

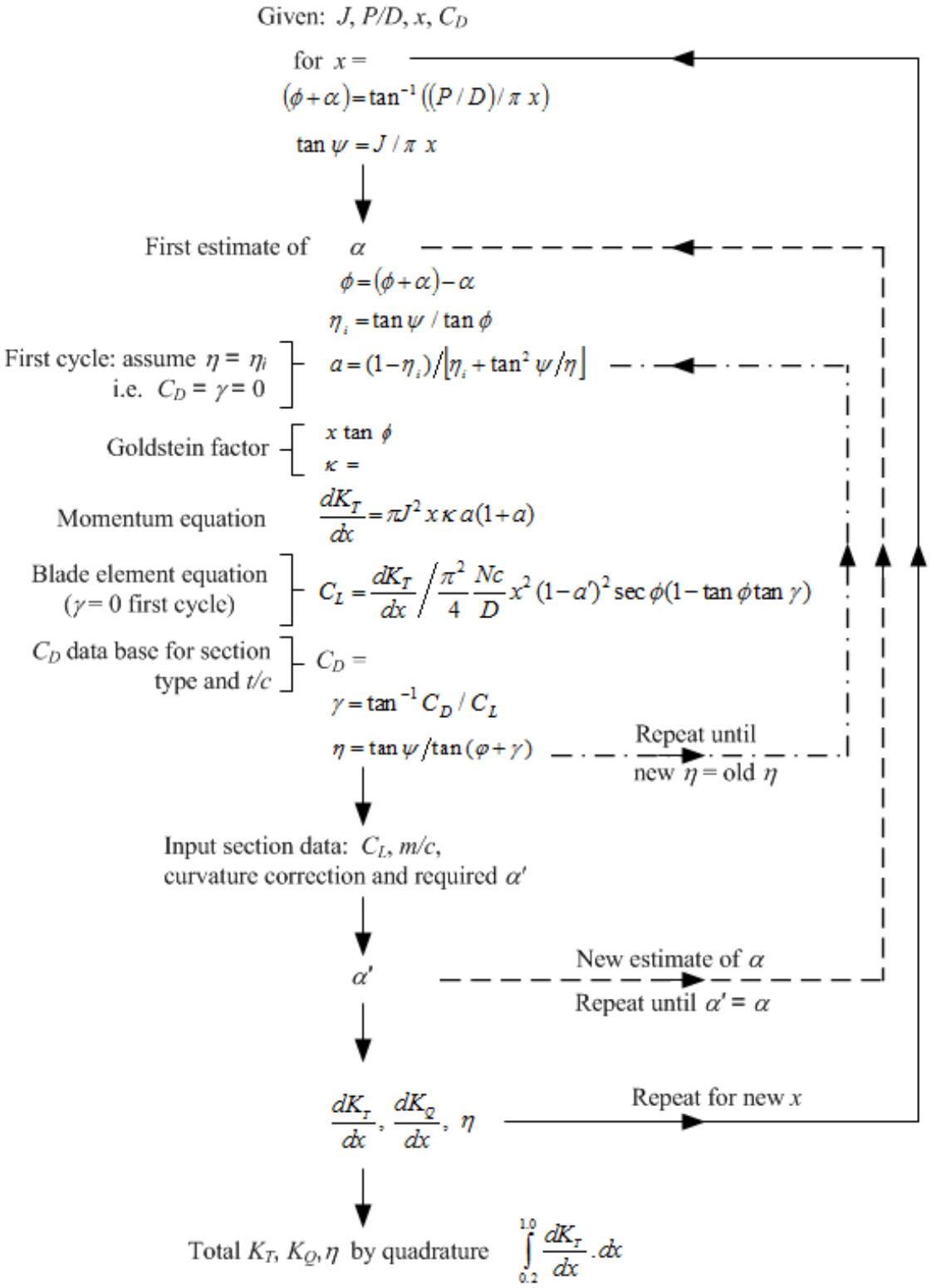

Figure 6: BEMT flow chart (Molland *et al.* 2011)

2.3 Theory of CFD

2.3.1 RANS derivation

The flow properties around most hull forms may be obtained by solving the Navier-Stokes equations. This set of equations is governed by three laws of conservation: mass, momentum and energy. Nevertheless, the incompressible nature of most fluid allows the elimination of the energy conservation.

The principle of conservation of mass, characterised by the continuity equation, states that the rate of change of mass in an infinitesimally small control volume is equal to the rate of mass flux through its bounding surface. In tensor notation, it may be expressed as:

$$\frac{\partial u_i}{\partial x_i} = 0 \tag{2.1}$$

The principle of conservation of momentum states that the rate of change of momentum for the infinitesimally small control volume is equal to the rate at which momentum is entering or leaving through buildingthe surface of the control volume, plus the sum of the forces acting on the volume itself.

$$\rho\frac{\partial u_i}{\partial t} + \rho\frac{\partial}{\partial x_j}(u_j u_i) = -\frac{\partial p}{\partial x_i} + \mu\frac{\partial}{\partial x_j}(\frac{\partial u_i}{\partial x_j} + \frac{\partial u_j}{\partial x_i}) \tag{2.2}$$

Combining equations 2.1 and 2.2 leads to the equations of motion of the incompressible Navier-Stokes equations:

$$\rho\frac{\partial u_i}{\partial t} + \rho u_j\frac{\partial u_i}{\partial x_j} = -\frac{\partial p}{\partial x_i} + \mu\frac{\partial^2 u_i}{\partial x_i \partial x_j} \tag{2.3}$$

Due to the highly turbulent character of the flow around a ship, the field properties (velocities and pressures) become random functions of time and space. They may then be expressed as the sum of mean and fluctuating properties as follows:

$$u_i = U_i + u_i^{'},\ p = P + p^{'} \tag{2.4}$$

$$\overline{u_i} = U_i,\ \overline{u_i^{'}} = 0$$

$$\overline{p} = P,\ \overline{p^{'}} = 0$$

The non-linear Navier-Stokes equations may then be simplified by introducing the concept of time-averaging. Substituting Equation 2.4 into 2.3 gives rise to the Reynolds-Averaged Navier-Stokes (RANS) equations.

$$\frac{\partial U_i}{\partial t} + U_j \frac{\partial U_i}{\partial x_j} = -\frac{\partial P}{\partial x_i} + \nu \frac{\partial^2 U_i}{\partial x_i \partial x_j} - \frac{\partial \overline{u_i' u_j'}}{\partial x_j} \tag{2.5}$$

The last term in the above equation includes the so-called Reynolds Stresses $\tau_{ij} = \overline{u_i' u_j'}$. These terms are responsible for the non-closure of the RANS system of equations (i.e. more unknowns than equations). As a result, the introduction of a set of equations known as a 'turbulence model' is required to solve the fluid properties.

2.3.2 Turbulence models

The most common approach is the Boussinesq hypothesis which relates the Reynolds stresses to the mean velocity gradients:

$$-\overline{u_i' u_j'} = 2\nu_T S_{ij} - \frac{2}{3} k \delta_{ij} \tag{2.6}$$

where:

k is the turbulent kinetic energy; $k = \frac{1}{2}\overline{u_i' u_j'}$ (KE/per unit mass)

ν_T is the kinetic eddy viscosity (Ns/m^2)

The most commonly used turbulence models include: Spallart-Allmaras, $k-\epsilon$, $k-\omega$ and Reynolds Stress models. The Spallart-Allmaras one-equation model is widely used in the aeronautic industry due to its ability to solve a single conservation equation (PDE) which contains convective and diffusive transport terms as well as terms defining the production and dissipation of the turbulent viscosity, ν_T. However, its use is limited to wall bounded-flow and as a result is not widely used for complex flows.

By introducing a second equation, the $k-\epsilon$ and $k-\omega$ turbulence models can be used to solve more complex flows such as the flow around a ship. The $k-\epsilon$ model describes the mechanisms that affect the turbulent kinetic energy. Using the RANS equations, an exact transport equation for the fluctuating vorticity and thus the dissipation rate, may be found to solve k and ϵ. Using the Kolmogorov-Prandtl expression, the turbulent viscosity may be solved as: $\nu_T = C_\mu \frac{k^2}{\epsilon}$ (Wilcox 2006). In the $k-\omega$ model, the turbulence

dissipation ϵ variable is replaced by 'the rate of dissipation of energy in unit volume and time parameter' (Wilcox 2006), ω. The first $k-\omega$ model was very basic and not fully developed as the understanding of turbulence was not completely understood. Since then, many modifications have been made to the $k-\omega$ model to improve its accuracy. Menter (1993) developed the Shear Stress Transport (SST) $k-\omega$ turbulence model. The increasing popularity of this model is due to the combination of the advantages of the $k-\omega$ and $k-\epsilon$ turbulence models; therefore it can be used for low and high Reynolds numbers. At low Reynolds numbers, it uses the $k-\omega$ model to solve the near wall region. In the free stream, where high Reynolds numbers occur, its characteristics become similar to a $k-\epsilon$ model.

2.3.3 Non-dimensional wall distance, y^+

To determine the resolution of a boundary layer mesh, a non-dimensional parameter, y^+, is used to define the distance between the wall and the centre of the first element in the mesh. Friction velocity defining y^+ is a function of shear stress and is used to describe the velocity profile on the wall. The non-dimensional wall distance, y^+, can be defined as:

$$y^+ = \frac{u_* y}{\nu} \tag{2.7}$$

where:

u_*(m/s): Friction velocity, $u_* = \sqrt{\frac{\tau}{\rho}}$

y (m): Distance from first grid point to the wall

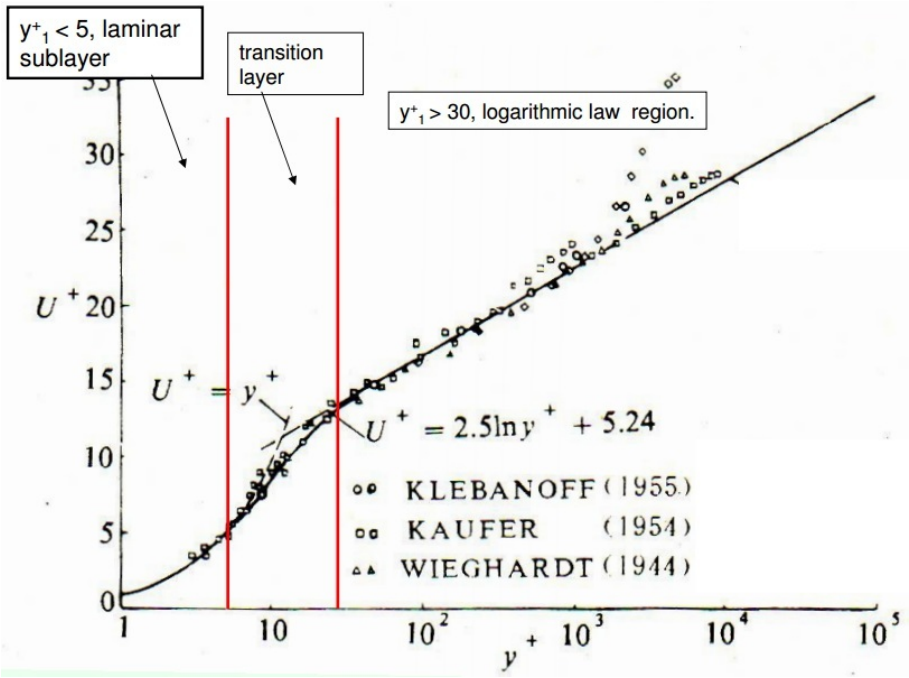

Figure 7: Velocity profile in the inner boundary layer (Schlichting 2000)

The value of y^+ determines in which region (laminar, transitional, turbulent) the boundary layer mesh is operating and thus allows one to choose the most appropriate turbulence model. The value of y^+ affects U_+, the non-dimensional friction velocity; and the subsequent operating region for a given mesh as shown in Figure 7. In the laminar sub-layer ($y^+ < 5$) the viscous stresses dominate the Reynolds stresses which may therefore be ignored. As y^+ increases ($5 < y^+ < 30$) the magnitude of the viscous and Reynolds stresses become comparable and hence neither may be ignored. As y^+ increases further ($y^+ > 30$) the Reynolds stresses become dominant and as a result the viscous stresses may be neglected.

This boundary layer characteristic affects how a turbulence model may be developed. Due to the flow complexity within the transition region, no turbulence model can accurately solve the flow. In the laminar sub-layer ($y^+ \sim 1$), the Spallart-Allmaras model would be used. However, the use of this model leads to a very fine boundary layer mesh and is thus not suitable to solve practical engineering problems where high Reynolds number flow may be found. In the turbulent region, the two-equation models are preferred. However, due to the increased y^+, the near-wall region in the boundary layer is not solved. As a result, wall-functions are introduced to model the near-wall region.

A typical CFD flow chart is shown in Figure 8 and is divided into three main steps:

- Pre-processing (set-up);
- Simulation (solution);
- Post-processing (interpretation).

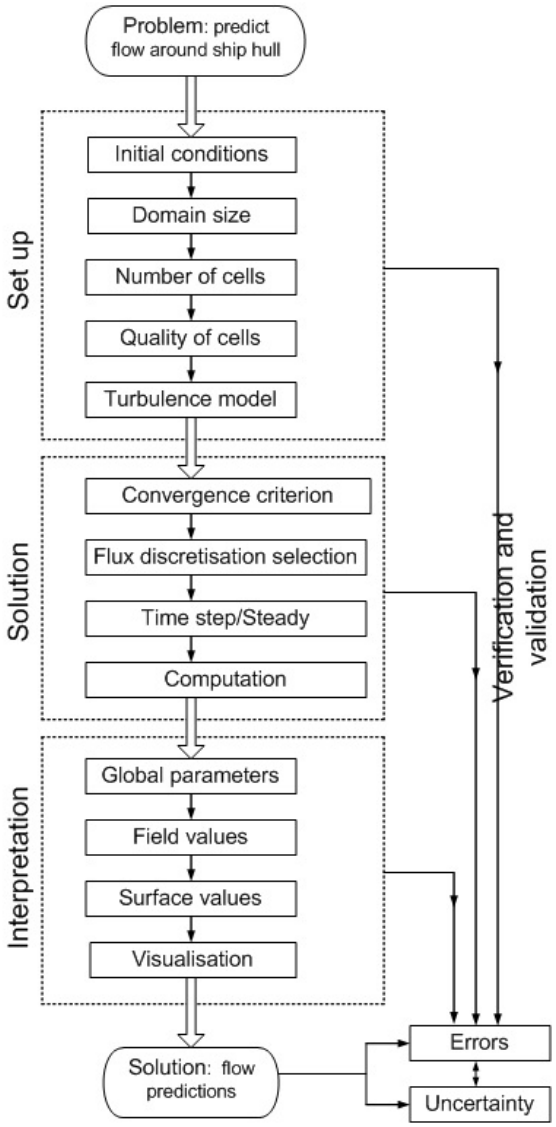

Figure 8: CFD process (Molland *et al.* 2011)

2.3.4 Free surface simulation - Volume of fluid technique

To model free-surface flows in CFD, two main techniques may be used: Lagrangian and Eulerian methods (Flow Science 2011). The Lagrangian methods are mostly suited for viscous and laminar flows. This method is relatively complex as the mesh moves to follow the interface shape. This mesh distortion may result in instability and internal inaccuracy. On the other hand, when using Eulerian methods, the fluid travels between cells without

any mesh distortion. This method is widely known as the volume of fluid (VOF) method. A factor is used to define the phase of each cell: α=0 for air and α=1 for the fluid. Around the free surface, where a cell may have both phases, the factor α will have a value ranging between 0 and 1. This will provide the height of the respective phases in each cell for a 2D problem. A similar process is adopted for 3D problems using multiple planes. Hence, using basic algebra and interpolation between the various planes, the free-surface parameters including local slope and curvature may be modelled. This will provide the solver with the 3D location of the free surface.

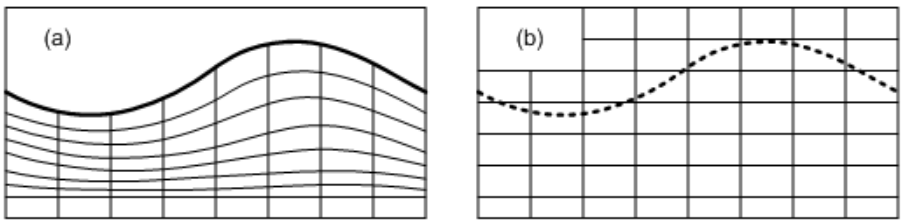

Figure 9: (a) Lagrangian mesh and (b) Eulerian VOF mesh (Molland *et al.* 2011)

When using a VOF method, a transient simulation is implemented for which an additional parameter known as Courant Number, C, is required (Courant *et al.* 1967). This type of simulation achieves convergence of the flow properties within a local time step, before proceeding.

Courant Number may be defined as:

$$C = c * \frac{\delta t}{\delta x} \tag{2.8}$$

where:

δt is the time step (s)

δt is the length interval (m)

In order to obtain realistic simulation including a free-surface, Courant Number should be between 0 and 1 (Courant *et al.* 1967). If $C \geq 1$, the solution becomes unstable and the results produced may be inaccurate. For a fixed wave celerity, Courant Number is proportional to the time step, δt, and inversely proportional to the length interval, δx. The easiest technique to reduce Courant Number is to decrease the time step, although this will increase the computational time in most cases. Alternatively, the cell size (δx) could be increased, resulting in a coarser mesh. In order to obtain a Courant Number

within its bounding limits (0 and 1), a compromise between computational time and mesh density must be found depending on the accuracy desired for the solution.

3 EXPERIMENTAL SET-UP

Experiments were carried out in the Mitchell Wind Tunnel at the University of Southampton. These experiments were used to validate the CFD simulations and allowed for an analysis of the existing naked hull form to be performed. The study of the naked hull was used as a benchmark to illustrate any flow changes observed in future investigations.

3.1 Benefits

Using wind tunnel tests offers two main advantages. First, the model scale factor can be smaller when compared to towing tank tests,resulting in a Reynolds number high enough to model a steady turbulent flow as experienced by the full scale ship. Furthermore, in a wind tunnel, wake pressure measurements are not affected by free surface effects (wave pattern).

3.2 Model Dimensioning

In order to accurately model the effect of retro-fit devices on the flow around the hull, it is important to ensure that the turbulent flow condition around the full scale ship is replicated at model scale. The onset of turbulent flow will occur, even on smooth bodies, when the Reynolds number exceeds 0.5×10^6 (Molland and Turnock 2007).

The Reynolds number of the full scale ship is calculated to be 1.187×10^9, confirming the need for turbulent flow around the experimental model. The 3.5m x 2.1m closed return Mitchell Wind Tunnel was used to its limit with a working section accepting models of upto 4m long and with a wind speed of 30m/s. The maximum achievable Reynolds number is 7.648×10^6.

Since only the stern flow is of interest in this investigation, the parallel mid-body is truncated as shown in Figure 10. This modification is made providing the flow without the parallel middle body is sufficiently similar to that required. It is in the assessment of this that CFD provides considerable use. A 4m model with a much smaller scale factor may thus be tested, reducing the magnitudes of the experimental and scaling errors.

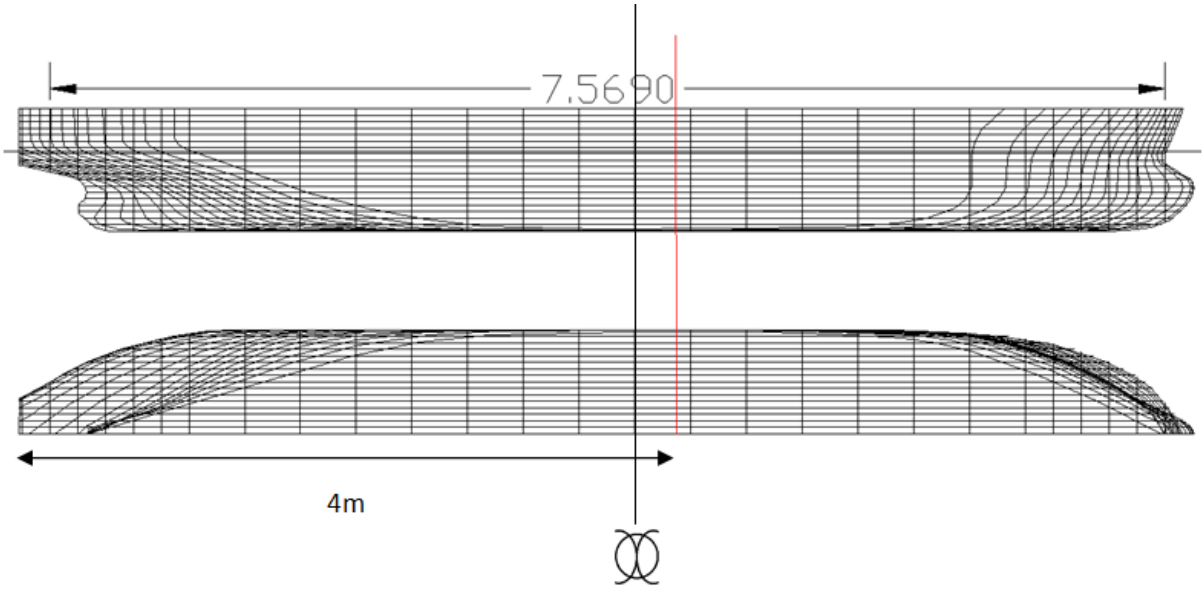

Figure 10: Truncated model length

The scale factor is calculated based on the assumption that at the propeller plane, the boundary layer thickness, δ (viscous wake), is approximately half of the propeller diameter. The boundary layer thickness is estimated, for the wrap around length of the 4m model, using the 1/7 power-law velocity distribution displayed in Equation 3.1 below:

$$\frac{\delta}{x} = 0.370 Re_x^{\frac{-1}{7}} \tag{3.1}$$

From these calculations the diameter of the propeller for the model is known and hence a scale of 1/23 is selected. For a 1/23 scale model, a blockage of 9.25% is created but still within the 10% limit where corrections may be applied. The dimensions of the wind tunnel model are summarised in Table 2. Table generated by Excel2LaTeX from sheet 'Sheet1'

Table 2: Wind tunnel model dimensions

		Ship	Model
Length, Over All	(m)	183.88	4.00
Breadth	(m)	32.2	1.40
Draught	(m)	12.416	0.54
C_B		0.8	-
Propeller Diameter	(m)	6.00	0.26
δ (at propeller plane)	(m)	1.40	0.14
% Blockage			9.25

3.3 Method of Wind Tunnel Testing

The wind tunnel experiments are aimed at recording pressures in the wake field and at the propeller plane of the truncated model. A traverse rig is used to move a Pitôt rake to the required locations. In addition, pressure tappings are employed to monitor that the flow reattached to the model at the stern despite the truncated bow. A schematic diagram of the set-up of the test may be seen in Figure 11.

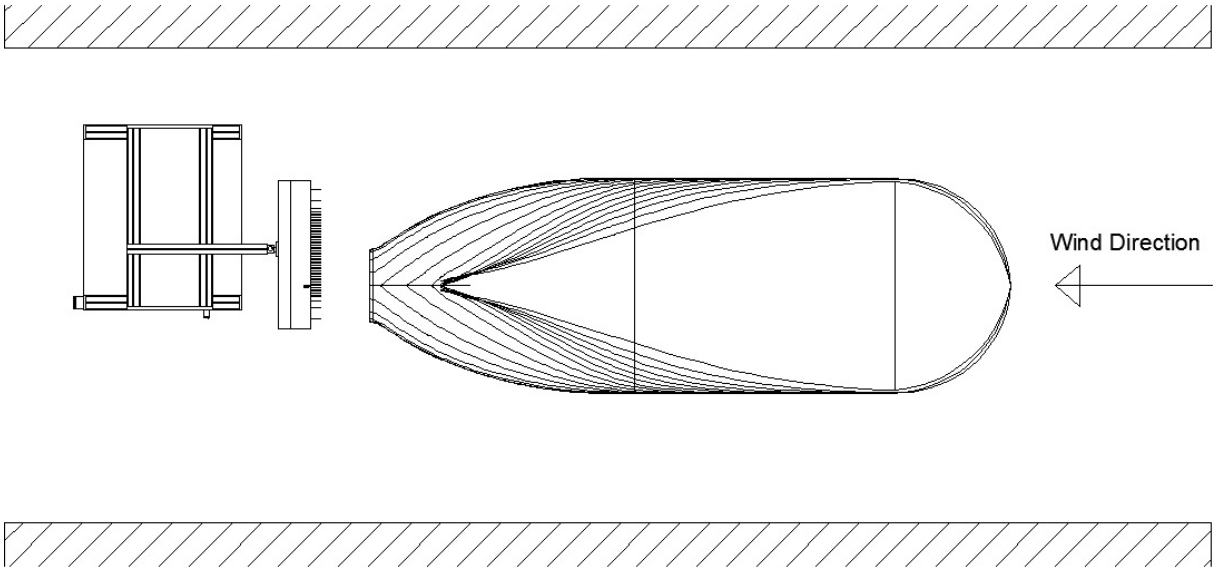

Figure 11: Wind tunnel test set-up with the wake traverse rig shown downstream of the model.

To qualitatively assess the flow pattern in the wind tunnel, tufts and an oil based paint are used. A matrix of x by y measurements is made at the desired plane using an

automated traverse. The recorded pressures in Pascals are converted into velocities using the simplified form of the incompressible Bernoulli's equation. For each test, the velocities are non-dimensionalised with the free stream velocity, U. Velocity contour plots are then generated at different planes at the stern.

The different appendages are compared based on the propeller efficiency. The blade-element momentum theory (Phillips et al, 2009) requires the wake fraction at specific locations int the propeller plane. As a result, a wake analysis is conducted. The Taylor wake fraction w_T is a measure of how the hull influences the velocity of the flow in the propeller region, and it may be expressed as:

$$w_T = 1 - \frac{u}{U} \tag{3.2}$$

4 NUMERICAL SET-UP

Computational Fluid Dynamics (CFD) was used to study the flow properties around the tanker hull form. A typical CFD process is divided into three main steps: pre-processing (set-up), simulation (solution), and post-processing (interpretation). The specifications for the CFD simulations in the wind tunnel and towing tank environments are presented in this section.

4.1 CFD for Wind Tunnel Tests

4.1.1 Pre-processing

4.1.1.1 Geometry In order to effectively simulate the wind tunnel experiments and to investigate the design of the retrofit devices, the initial conditions of the CFD simulations were carefully chosen. This allowed the simulation to be completed in a practical time, without detrimentally effecting the accuracy of the results.

Before any simulation set up could be completed, the geometry of the truncated hull form tested in the wind tunnel was required. To import the geometry into OpenFOAM, a .stl file was generated from Rhinoceros. The quality of the geometry greatly affects the mesh generation process. This occurs as the resolution of the mesh on the geometry cannot be greater than the number of panels used to define the geometry.

4.1.1.2 Domain size The domain size was based on the wind tunnel dimensions. The cross section of the wind tunnel (3.5m wide x 2.6m high) was applied such that the same blockage effect encountered by the model in the experiments was computationally modelled. However, due to the complexity of the wind tunnel, only the working section length was incorporated within the simulation. Therefore, the initial domain length was 1.5L upstream and 3L downstream relative to the model. To determine the effect of this assumption a domain analysis was completed, see below Section 5.1.

The boundary conditions applied to the domain and geometry were chosen in a similar manner to the domain size. The inlet and outlet boundary field types were defined as a fixed velocity inlet/outlet respectively (U = 30m/s). The hull form was defined as a non-slip wall, and the upper and side walls were given a slip condition. The effect of the slip condition was deemed to have a negligible effect on the flow around the model, when compared to the experimental results. The bottom wall was defined as a symmetry wall,

as it can be used to simulate the free surface effect within the wind tunnel environment. This condition could only be applied due to the boundary layer removal system installed in the wind tunnel.

4.1.1.3 Mesh generation The quality of the mesh used in CFD simulations is one of the most important factors to obtain accurate results. In general, the greater number of elements, the more accurate the results will become. However, as the number of elements increases, the computational time increases. Consequently, a compromise is required between number of elements and computational time. With a pre-determined understanding of the flow physics in a simulation, a high quality mesh can be created. This occurs as a concentration of elements may be placed in areas which allow the flow to fully develop, for example around the bilge of a hull form to effectively simulate bilge vortices.

There are two main types of mesh: structured and unstructured. A structured mesh consists of a set of coordinates and connections that naturally map into elements of a matrix. On the other hand, no mesh structure is required for an unstructured mesh and the (i,j,k) ordering of points is non-existent. A structured mesh is preferred as it requires fewer elements than an unstructured mesh to produce a solution with a similar level of accuracy. However, an unstructured mesh has the ability to create high quality mesh zones around complex geometries with a relatively low level of expertise. The method used in OpenFOAM is a hybrid technique where a structured boundary layer mesh is surrounded by an unstructured domain mesh.

A mesh in OpenFOAM is generated using two separate utilities: blockMesh and snappyHexMesh. The blockMesh utility is used to create a simple hexahedral mesh extending to the limits of the domain. The number of elements in the x,y,z directions are chosen such that the height, width and depth of each element are equal; these dimensions are known as the base size. The elements should be defined in this manner to allow the snappyHexMesh snapping function to accurately define the mesh around the imported geometry.

The snappyHexMesh utility is the second meshing tool used in OpenFOAM. This utility uses the blockMesh to generate the final mesh used in the simulation. The final mesh is created by systematically progressing through three separate functions: castellatedMesh, snap and addLayers.

The castellatedMesh is the initial step which refines the blockMesh in defined areas of interest. The function uses simple geometries, such as boxes and cylinders, to define the refinement regions. Additionally, refinement is conducted at defined levels and distances away from the surface to ensure a smooth growth rate of element size (from the geometry to the blockMesh base size in the outer domain), as shown in Figure 12. Subsequently, the process advances onto the snap function, where elements are removed and split along the surface of the geometry. Using an iterative process, the surface of the geometry can be accurately defined (Figure 13). The final step is where the layer addition function creates a boundary layer mesh on the surface of the geometry (Figure 14). A boundary layer mesh is vital to effectively simulate the development of a boundary layer along a hull form and to capture the viscous flow.

The parameters of the boundary layer mesh are therefore complex and must be carefully chosen. These parameters depend on the desired y^+. The dimensional wall distance, y, used to control the addLayers function, was derived as below.

The skin friction coefficient is defined using the 1957 ITTC formula:

$$C_F = \frac{0.075}{[\log Re - 2]^2} \tag{4.1}$$

The wall shear stress may then be express as:

$$\tau = \frac{1}{2}\rho U^2 C_F = \rho {U_*}^2 \tag{4.2}$$

The friction velocity, U^*, may then be obtained by re-arranging Equation 4.2. Hence, the dimensional distance to the wall, y, may be determined as:

$$y = \frac{2y^+\nu}{u^*} \tag{4.3}$$

The final layer corresponds to the outer layer of the boundary layer mesh. Its thickness is dependent upon the dimensional wall distance, the boundary layer ratio ($\delta^{'}$), the expansion ratio (expr) and the number of layers (N)(Banks 2010). The boundary layer ratio and the expansion ratio are assumed. The boundary layer ratio ($0.5 \leq \delta^{'} \leq expr$) is used to define the final layer thickness of the mesh and its value is varied to ensure the transition from the boundary layer mesh to the domain mesh is smooth. Similarly, the expansion ratio defines the growth rate of the boundary layer mesh. The value of these parameters cannot be calculated; however, they can be assumed using prior knowledge of mesh generation.

The number of layers is defined by:

$$N = \log_{expr}[\frac{\delta^{'}}{y^{'}}] + 1 \tag{4.4}$$

$y^{'}$ is defined as the ratio between the wall distance y and the base size on the stl, where: Base size on the stl = Base size/2^{x} (x = level of refinement).

The final layer thickness may then be obtained as:

$$\delta = \frac{y[1 - expr^{N}]}{1 - expr} \tag{4.5}$$

4.1.1.4 Wind tunnel model: Mesh particulars The mesh for the wind tunnel model was generated using two additional refinement cylinders located on each bilge keel and one refinement box located at the aft section of the hull form. These regions were chosen as key areas to refine the mesh as the flow around the bilges and the stern could be correctly captured. The boundary layer mesh parameters were selected for a y^{+} value of 30 and a minimum total thickness of 8mm (based on flat plate theory). This was achieved with a boundary layer thickness ratio of 0.62, an expansion ratio of 1.3 and seven layers. The whole mesh is shown in Figure 15.

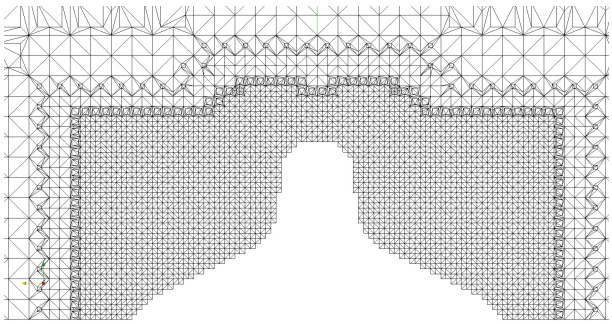

Figure 12: Castellated mesh

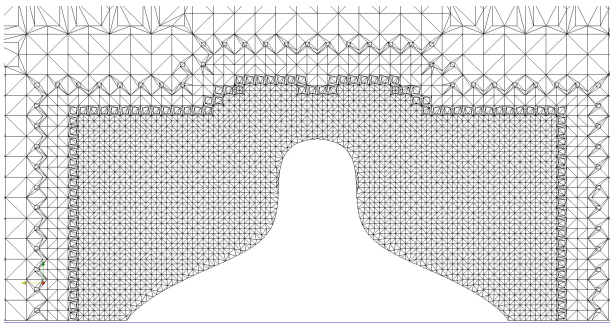

Figure 13: Snap feature

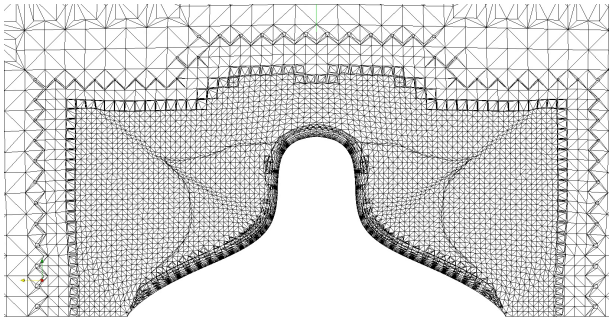

Figure 14: Layer addition process

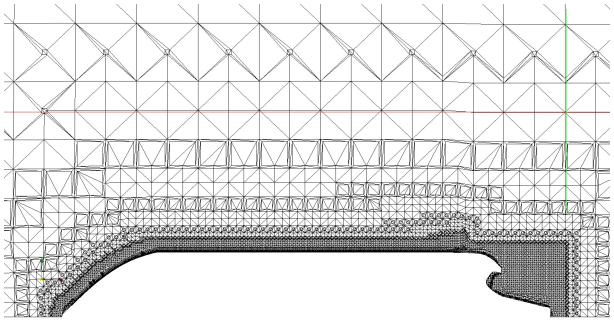

Figure 15: Final mesh along the x-direction

Overall, the quality of the mesh is reasonably good with just over one million elements. The parameters used to define the boundary layer mesh provide a 99.5% extrusion success. Figure 15 shows a smooth growth rate across the domain, allowing accurate interpolation of the field properties between elements. However, the thickness of the inner refinement level should ideally be reduced to limit the element counts without vastly compromising the accuracy of the solution. This could not be completed due to the inability to further refine the inner level with the available computational resources.

The parameters used to obtain this mesh were considered to be a good compromise between mesh quality and number of elements. Consequently, these conditions were maintained to perform future mesh generations for the wind tunnel study.

4.1.2 Simulation

The flow around a tanker hull form can be simulated using a steady-state solver. The OpenFOAM solver simpleFoam was chosen for this study of the wind tunnel model (single phase). This solver is based on a Semi-Implicit Method for Pressure-Linked Equation (SIMPLE) and uses a pressure correction. The flow properties are solved until the predefined convergence criteria are met (10^{-6} - Good convergence).

Since this study is based on a RANS simulation, the SIMPLE algorithm requires a turbulence model. The $k-\omega$ SST model was found to be the most appropriate.

4.1.3 Verification and Validation Studies

In order to verify CFD simulations, several analyses may be performed: y^+ value, domain analysis, mesh dependency study and turbulence model analysis. Initially, the y^+ value was checked to ensure compatibility with the chosen turbulence model, $k-\omega$ SST. y^+ is required to lie between 30 and 250. As shown in Figure 16, this criterion was largely met. Regions where y^+ is greater than 300 have a negligible effect on the results.

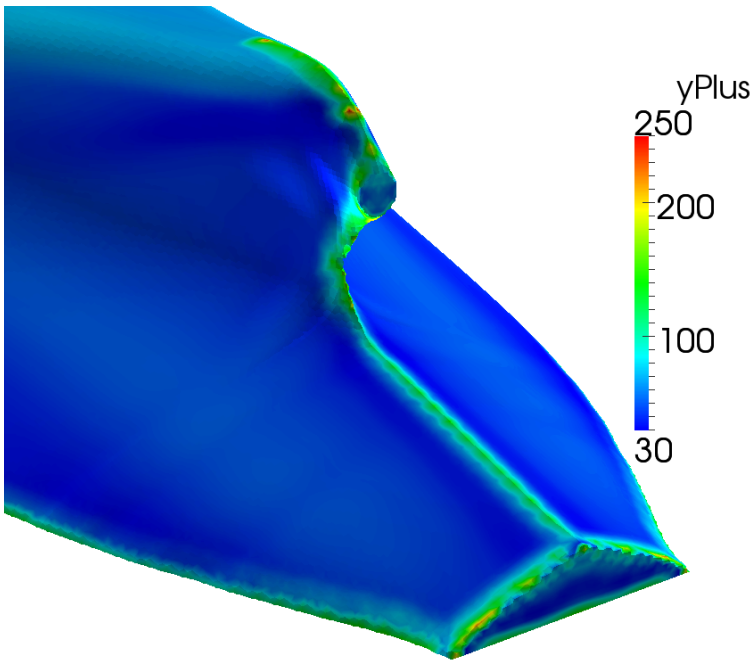

Figure 16: y^+ distribution at the stern

In addition, a domain analysis was conducted. Since the width and height of the domain were restricted (wind tunnel cross-section), only the effect of the domain length was assessed. By systematically doubling the domain length both upstream and downstream, three domains were compared based on the efficiency output from the BEMT code, η_{BEMT}. The percentage difference is negligible (Table 3); hence the domain length used for all further simulations was set to 1.5L upstream and 3L downstream.

Table 3: CFD verification: domain analysis

	Element no.	**L downstream**	**L upstream**	η_{BEMT}	$\Delta\eta_{BEMT}$
		(m)	**(m)**		**(%)**
Domain 1	1 036 970	3	1.5	0.6821	**-**
Domain 2	1 038 090	6	3	0.6816	**0.07**
Domain 3	1 040 330	10	6	0.6815	**0.09**

The next step in the validation process was to undertake a mesh dependency study to determine the limiting number of elements required to obtain a reasonably accurate solution. The refinement process was completed using a systematic approach. The base size was multiplied by a factor of $2\sqrt{2}$ repetitively until a desired mesh resolution was achieved (greater than 10 million) without modifying the boundary layer mesh. Five

different mesh resolutions were generated. The efficiency output from the BEMT code was used to compare each mesh (Table 4). The efficiencies obtained for each mesh are within the error band of the wind tunnel experiment as shown in Figure 17. This proves that all the generated meshes have a sufficient resolution to achieve convergence of the results. In conclusion, the coarse-medium mesh is suitable for all the wind tunnel cases. However, in order to perform a complete mesh dependency study, an even coarser mesh should be generated. The aim is to determine the limiting number of elements to be used to reach convergence of the results.

Since most of the velocities are probed in the boundary layer region, it is important to study the effect of the mesh in this region. Indeed, varying the boundary layer mesh would affect the y^+ value, and would thus require a different turbulence model. To complete an extensive verification study, alternative turbulence models could be used while retaining the same y^+ value. However, due to the time constraint of this project, this is left as further work.

Table 4: Naked hull mesh dependency results

	Element count	η_{BEMT}	$\Delta\eta_{BEMT}$ (%)
Wind Tunnel Test 1	**-**	0.6188	**-**
Wind Tunnel Test 2	**-**	0.7033	**-13.66**
Coarse mesh	705 541	0.6806	**-9.99**
Coarse-medium mesh	1 036 970	0.6821	**-10.23**
Medium mesh	1 778 934	0.6634	**-7.21**
Medium-fine Mesh	4 353 463	0.6965	**-12.56**
Fine Mesh	11 515 963	0.6680	**-7.95**

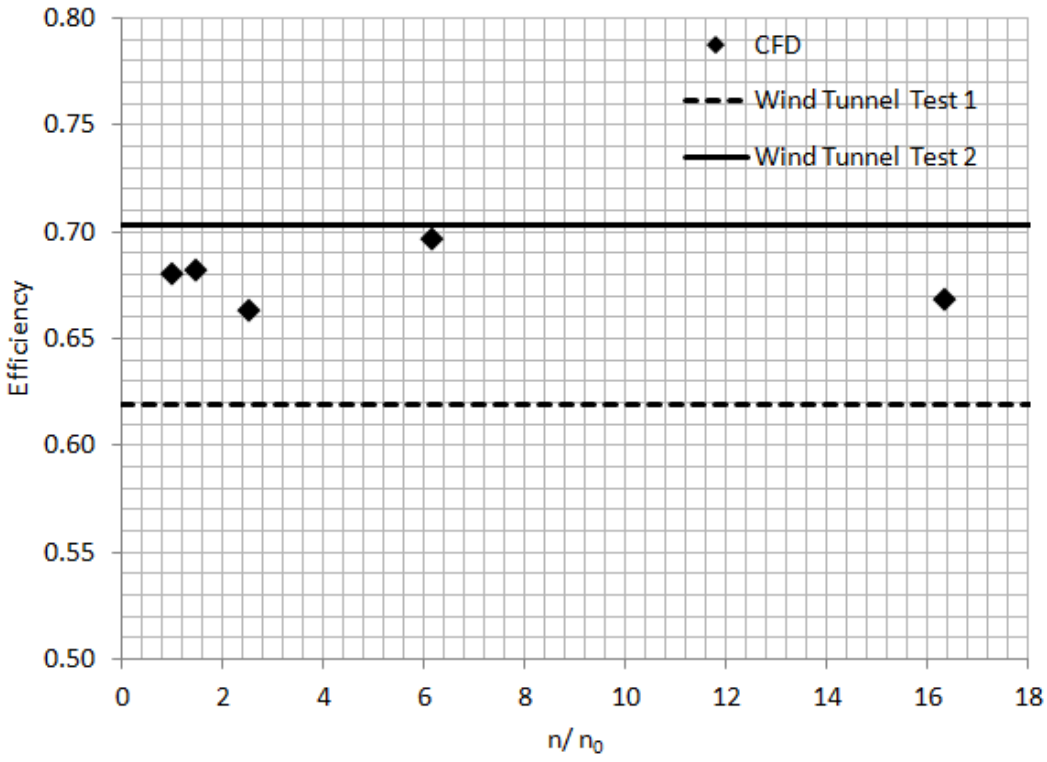

Figure 17: Mesh dependency study based on η_{BEMT}, where n_0 is the number of elements of the coarsest mesh

5 NAKED HULL RESULTS AND ANALYSIS

Following the analytical and experimental techniques performed, using the naked hull, the results are presented and discussed.

5.1 CFD post-processing

There are various techniques available to analyse results from a CFD simulation:

- Streamlines;
- Velocity vector plots;
- Contour plots (velocity/pressure);
- Extraction of local velocity and pressure components (probing, sampling).

The flow pattern was initially analysed using streamlines. To quantify the results, the local axial velocities were extracted at the propeller plane to form the wake matrix used in the BEMT code. Moreover, velocity components were probed over the entire propeller plane and further aft in the wake field. Using the visualisation tool 'Paraview', contour plots could then be generated allowing a direct comparison with the wind tunnel test results (Section 5.3).

5.2 Effects of truncation

5.2.1 Wake radial distribution

The effect of the truncation of the parallel midbody was studied based on the radial distribution of the wake obtained from the CFD simulations. The radial wake fraction may be expressed as:

$$w_T{}' = \frac{1}{2\pi}\int_0^{2\pi} w_T{}'' d\theta \tag{5.1}$$

where: $w_T{}''$ is the axial wake component; $w_T{}'$ is the radial distribution of the wake.

A comparison between the wind tunnel model (truncated âĂŞ L=4m) and the non-truncated model (L=8m) for identical Reynolds number is presented in Figure 18. In addition, a simulation of the non-truncated model with a matching Reynolds number to the full scale ship was completed.

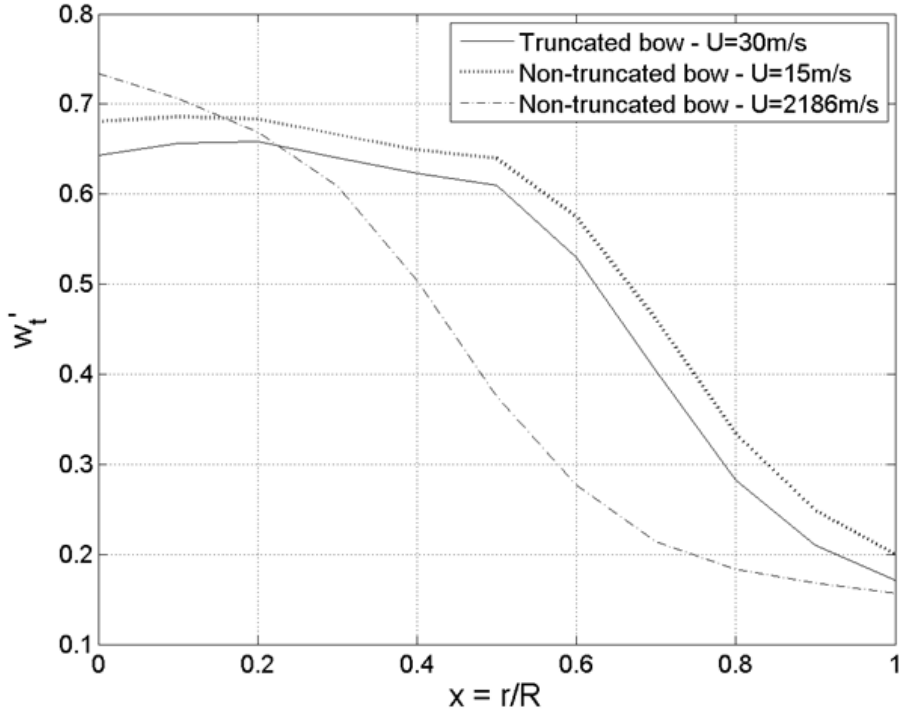

Figure 18: Effect of truncation: wake radial distribution

Table 5: Effect of truncation: nominal mean wake

	Nominal wake, w_T
Truncated model - U = 30m/s	0.3987
Non-truncated model - U = 15m/s	0.4386
Non-truncated model - U = 2186m/s	0.2773

Table 5 shows that the effect of truncation on the flow field is negligible. However, a model scale simulation where the Reynolds number is matched to the full scale ship still induces scaling errors, as the boundary layer thickness does not vary linearly with Reynolds number. The use of oversized devices is therefore required to counteract this effect. ***Pressure tappings***

5.2.2 Pressure tappings

As well as affecting the boundary layer thickness, truncation of the model is likely to affect the flow separation around the model. Similarity of the flow around the truncated model and the full size ship is essential to ensure the validity of the study, since devices fitted onto

the side of the hull, such as vanes, will yield very different results depending on whether the flow is attached or separated from the hull. The effect of truncating the model on the flow over the model therefore needed to be analysed to verify that the truncation did not lead to separation, which would not be seen on the full size ship. Although a certain amount of separation ahead of the point where the devices are to be fitted is tolerable, it was very important that the flow had reattached by the time the vanes were reached. A CFD plot of the expected pressure distribution was obtained (Figure 19).

Figure 19: Pressure distribution on hull as predicted by CFD

As can be seen from this plot, separation (areas of lower pressure, shown in blue in Figure 19) does occur just aft of the truncated bow but only for a small area before the flow reattaches, as confirmed by the slowly increasing pressure with distance towards the stern. Indeed, a slowly increasing pressure confirms that the flow is being affected by the presence of the curved hull, suggesting it is attached to the hull. Figure 19 therefore confirmed the suitability of using a truncated model. However, experimental validation of the CFD was still required. Pressure tappings were therefore placed on the hull to check the pressure distribution on the model.

Pressure tappings consist of metal tubing of approximately 20mm in length and 1.2mm internal diameter, connected to PVC tubing which in turn is connected to the Scanivalve box described earlier in this report. The metal tubes were fixed onto the model using super glue, such that the end of the tube was flush with the model surface.

The CFD pressure distribution plot suggested separation occurred in the area directly astern of the truncated bow. A row of tappings was therefore placed in this region to help validation. Rows were then placed further aft to verify the flow was not separating around where the vanes would be positioned. Analysis of the first sets of result highlighted the

need for an intermediate row to be placed to get a clearer idea of the pressure variations in this region. The lack of tubing available only allowed for five more tappings to be placed on the model. These were placed on the side of the hull, which is the area of interest considering the vanes are also fitted to the side of the hull.

The majority of the measurements were taken on the port side of the hull in a similar manner as the wake traverse measurements. A limited number of tappings were placed at varying z locations on the starboard side as a means of verifying symmetry of the flow separation patterns recorded. The pressure distribution was measured over six runs and averaged to obtain the final pressure distribution shown in Figures 20 and 21.

As can be seen from Figures 20 and 21, the pressure generally increases from the fore to the aft of the model suggesting separation has not occurred. The general trend therefore mirrors the CFD predictions. Furthermore, the area of very low pressure just behind the bow, which was predicted by CFD, is also seen on the plot at X= 3.15m. However, the experimental data shows a sudden increase in pressure on some parts of the hull at X=1.78m, suggesting the flow velocity significantly decreases at this point, before re-accelerating to yield negative pressures at X=1.47m. Such accelerations could be due to a lack of fairing of the model around this area which may cause minimal amounts of separation. The relative lack of port-starboard symmetry in the pressure readings (as shown in Figures 20 and 21) seems to confirm that irregularity in the local fairing exists.

Nevertheless, the flow is likely to have re-attached by the time it reaches the device, the forward most point of which is located at X=1.58m.

Further validation of the CFD prediction was carried out by direct comparison of the pressure values. The magnitudes of the perwaiting on the new figurescentage difference values in suggested poor agreement between CFD and experimental results. Further work would therefore be required in the CFD modelling to obtain more accurate pressure readings. However, due to the comparative nature of the investigation, the similarity in general trends shown in the experimental and CFD data is enough to validate the CFD and confirm that flow separation does not occur over the model surface.

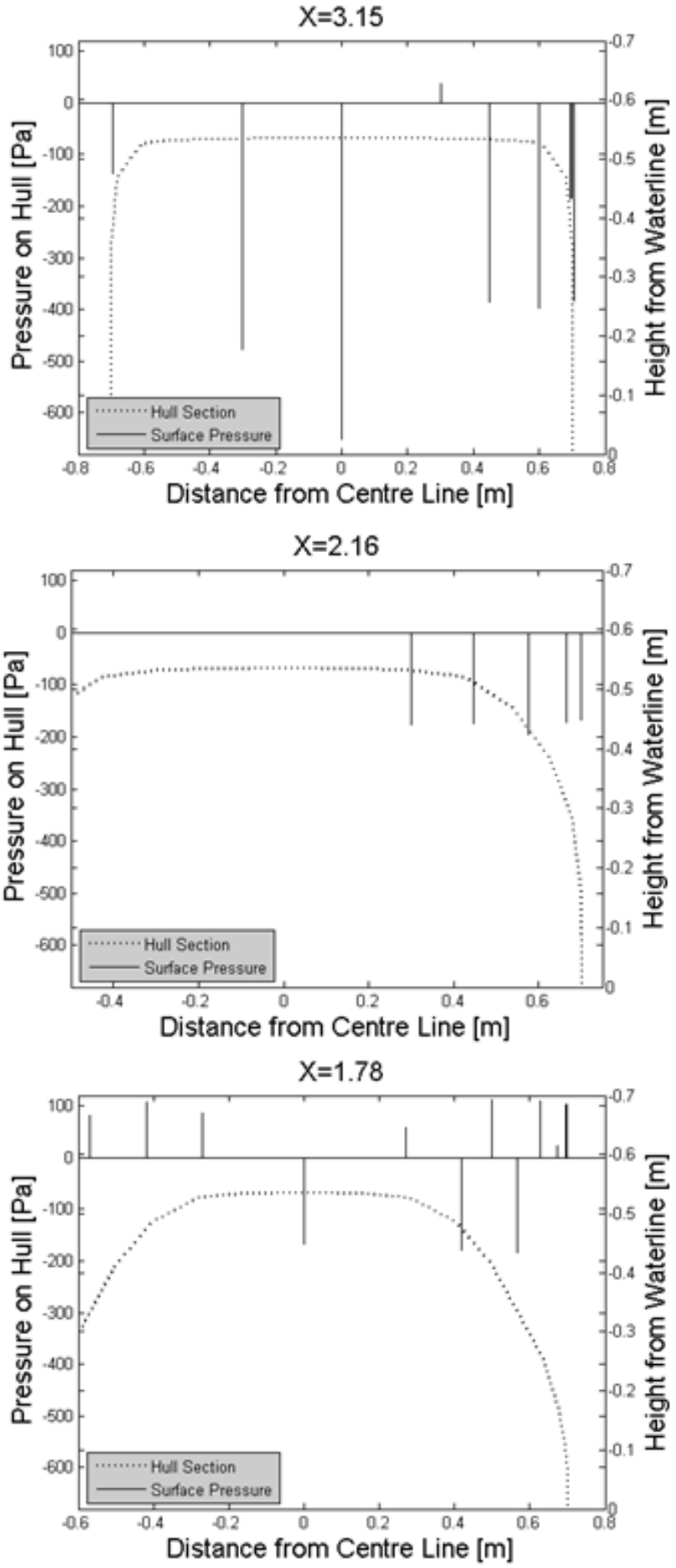

Figure 20: Results from forward pressure tappings

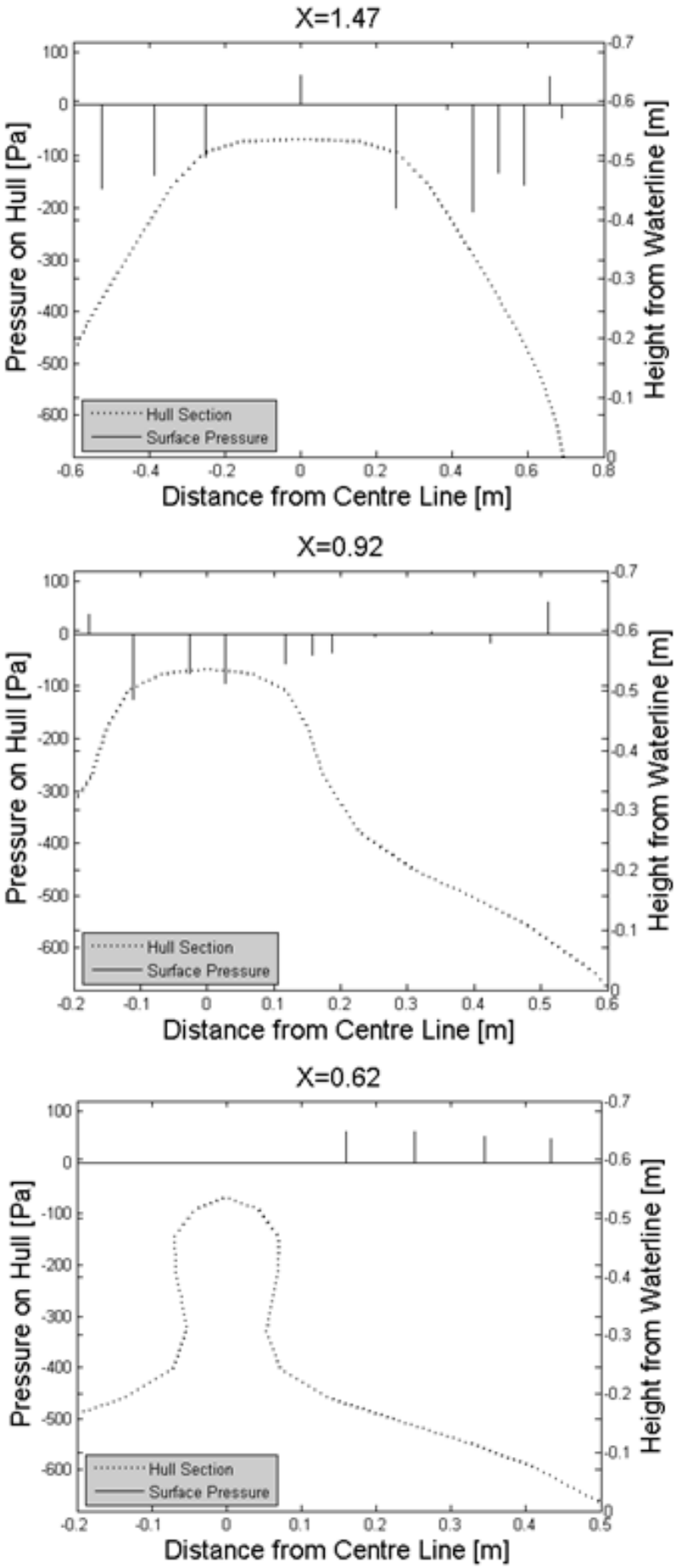

Figure 21: Results from aft pressure tappings

5.3 Flow and wake fields

The flow pattern was identified using streamlines in CFD and an attempt was made to validate the CFD results in the wind tunnel using oil based paint and tufts, as shown in Figures 22, 23 and 24. The oil based paint flow visualisation was unsuccessful in the second wind tunnel test. Due to the increased temperature in the wind tunnel, the brush marks obscured the flow visualisation.

A clear similarity between the flow patterns was observed, suggesting that the flow is diverted away from the propeller plane. Indeed, this first impression was confirmed upon examination of the contour plots shown in Figures 25 and 26. The propeller operates in the region where the flow is slowest, whereas for increased efficiency, it is desirable for the flow into the propeller to have a higher velocity. The figures also confirm that the CFD and wind tunnel wake plots are similar, although the mid-wake obtained in the wind tunnel does seem to be wider and higher than that predicted by CFD. Furthermore, the CFD does not seem to predict the small gradual changes in velocity which can be seen in the experimental wake both in the Y direction (at the propeller plane) and in the Z direction (at the mid-wake). These differences are likely to explain the discrepancies in efficiency values shown in Table 6. Indeed, when operating in the CFD generated wake, a much greater proportion of the propeller blade is located in the lighter grey region of faster flow, whereas when operating in the experimental wake, the propeller operates in a region of slower flow which gradually increases to the velocity predicted by CFD.

Considering the likely sources of experimental error, combined with the percentage tolerances of the CFD, a difference in efficiency of just over 9% was judged to be acceptable when comparing predictions obtained from computational and experimental methods. This, together with the similar general trends obtained both in wake and hull flow fields, suggests that the CFD simulation has been validated by the wind tunnel results. develop discussion - expand on percentage error - be critical

The CFD simulation can therefore be used to accurately analyse the effect of various devices on the wake field and propeller efficiency.

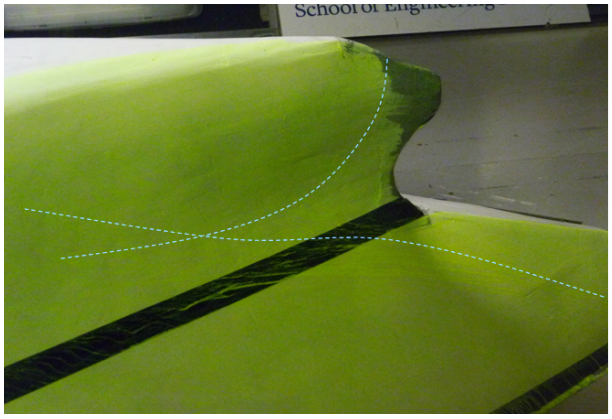

Figure 22: Flow streamlines on the wind tunnel model

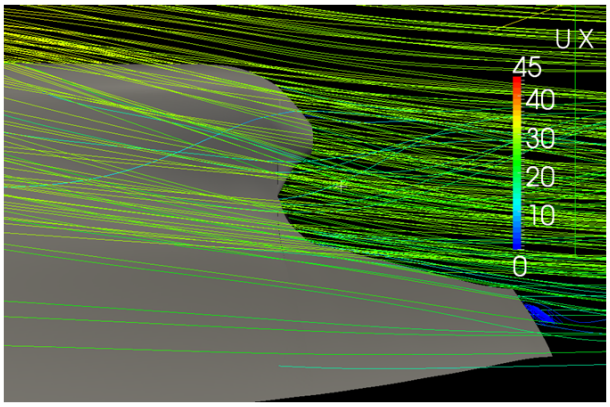

Figure 23: Flow streamlines on the model generated by CFD

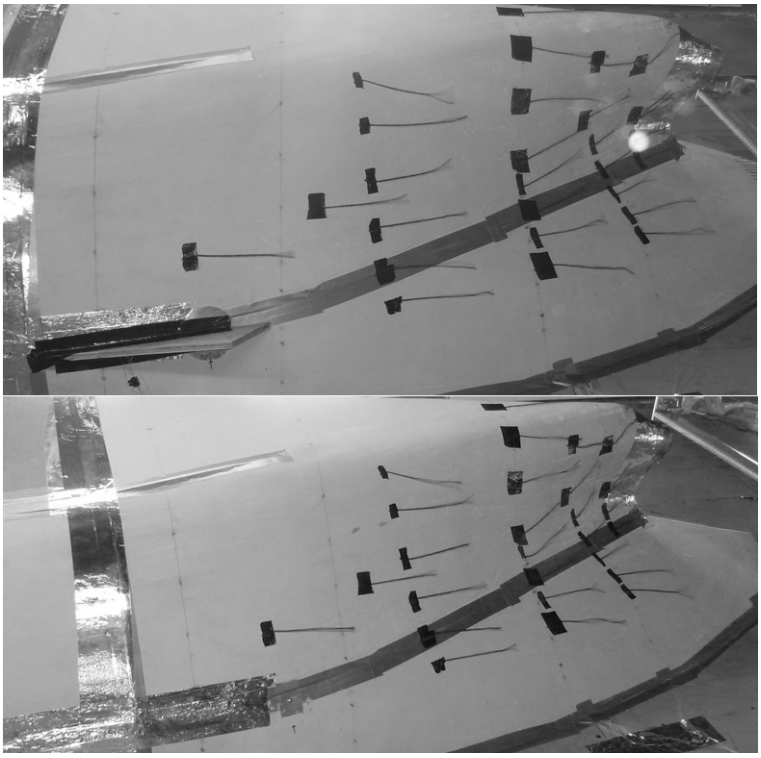

Figure 24: Flow over the stern due to device (top) and for the naked hull (bottom)

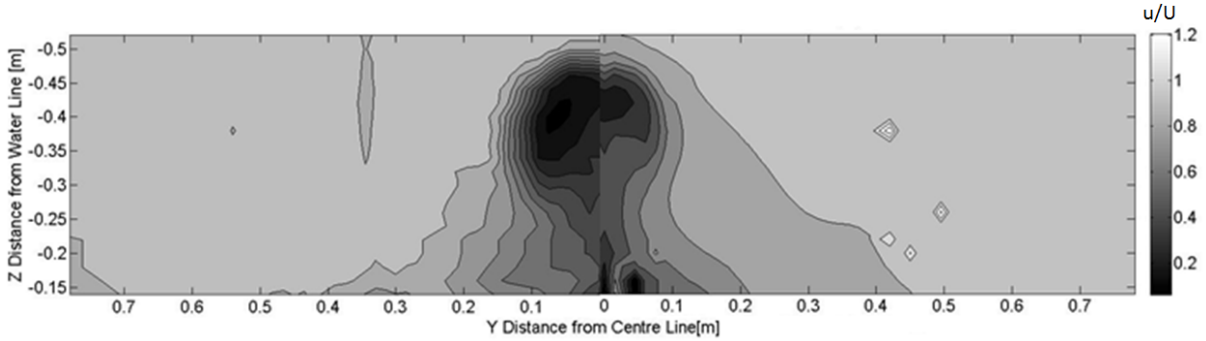

Figure 25: Propeller plane contour plots of wind tunnel test 1 (left) and CFD (right)

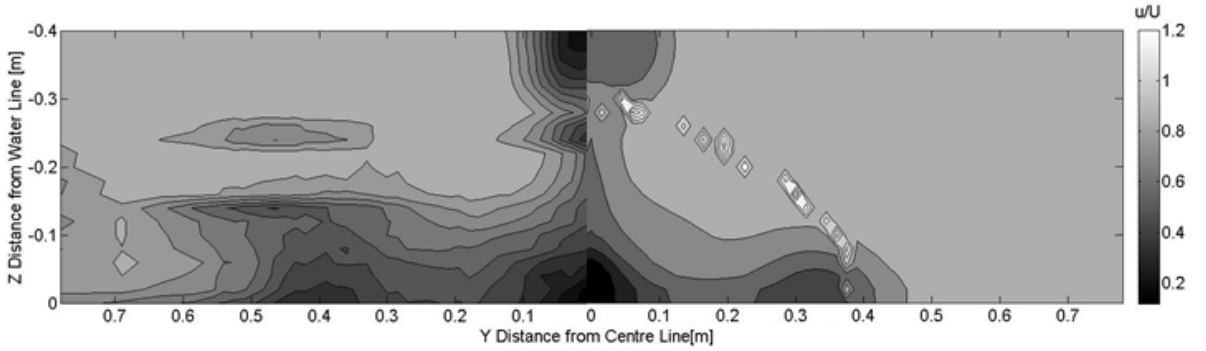

Figure 26: Mid-wake contour plots of wind tunnel test 1 (left) and CFD (right)

Table 6: Naked hull results - comparisons of wind tunnel efficiencies against CFD predictions

	K_T	K_Q	η_{BEMT}	$\Delta\ \eta_{BEMT}$ (%)
CFD	0.1920	0.0229	0.6821	-
Wind Tunnel Test 1	0.1167	0.0153	0.6188	9.28
Wind Tunnel Test 2	0.1055	0.0146	0.7033	-3.11

6 INVESTIGATION OF DEVICES

A large range of possible device designs and locations were tested in CFD. From this, an initial vane configuration was recommended to be further tested in a towing tank environment.

6.1 Design of devices tested in CFD

Based on the initial study of the flow pattern around the naked hull and the research on current retro-fit devices, two main types of devices were retained: vortex generating fins and flow channelling ducts. Since the flow appeared to be diverging away from the propeller plane, it was decided to position a vortex generator upstream (see Section 5) in order to redirect the flow with an increased velocity. Fins with varying parameters of location, angle and shape were designed and tested in CFD to analyse their effects on the flow field. Two fins were designed based on a triangular shape and several angles were tested (Figures 27 and 28).

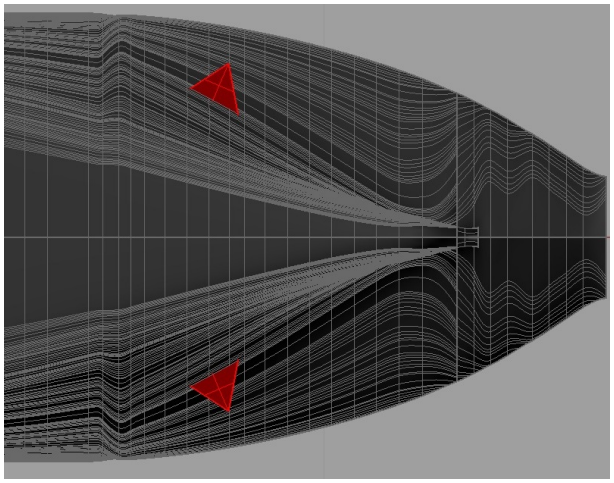

Figure 27: Vane 1 - [200, 150, 20] (mm)

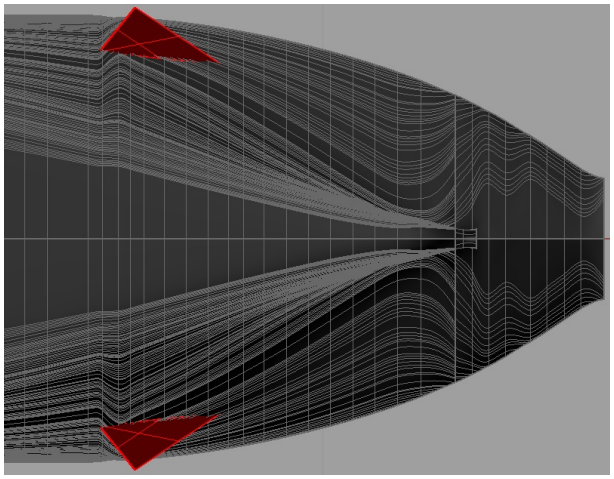

Figure 28: Vane 2 - [400, 150, 12] (mm)

Figure 29: Convention for fin angle rotation

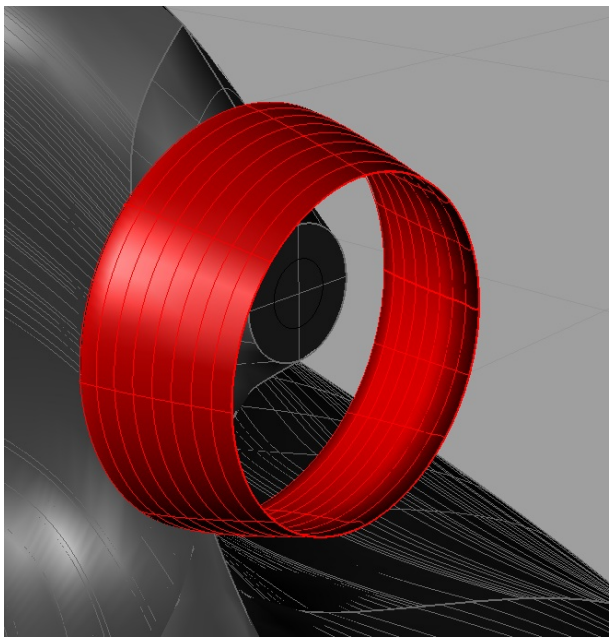

Figure 30: Duct

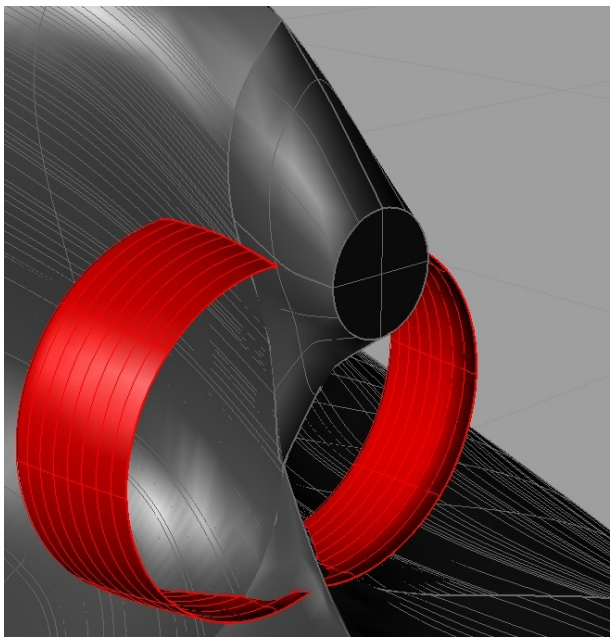

Figure 31: Wake equalising duct

Two types of duct were studied: Mewis (Figure 30) and wake equalising ducts (Figure 31). The duct design was based on Mewis (2009) and a NACA 0006 section was assumed. Different ratios between inlet and outlet diameter were tested.

6.2 Results

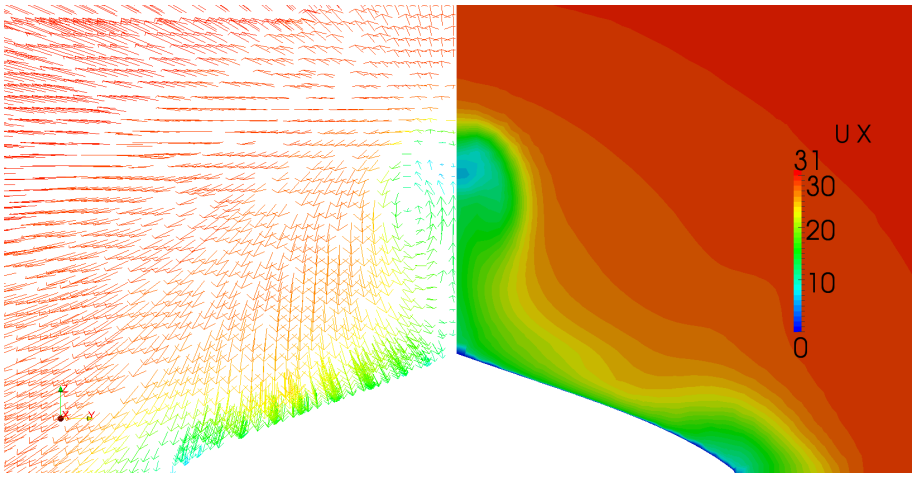

Figure 32: Naked hull at propeller plane: velocity vectors and contour plot

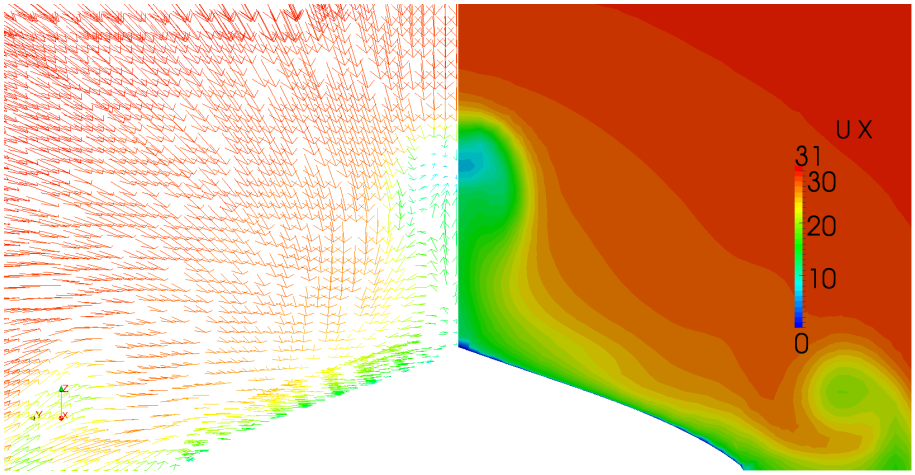

Figure 33: Device 5 at propeller plane: velocity vectors and contour plot

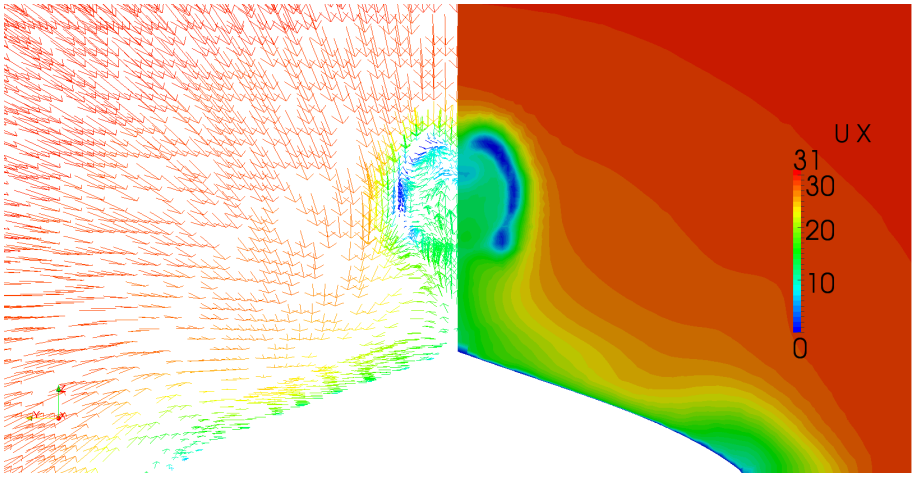

Figure 34: Device 8 at propeller plane: velocity vectors and contour plot

Table 7: Comparison of potential retro-fit devices

Retrofit devices tested	K_T	K_Q	η_{BEMT}	w_T
CFD naked hull	0.1920	0.0229	0.6821	0.3987
Wind tunnel naked hull	0.1167	0.0153	0.6188	-
1 - CFD Vane 1: 0 deg	0.1827	0.0221	0.6852	0.3632
2 - CFD Vane 1: +10 deg	0.2006	0.0239	0.6007	0.4305
3 - CFD Vane 1: -10 deg	0.1881	0.0226	0.6874	0.3849
4 - CFD Vane 2: -15 deg - t=20mm	0.1889	0.0226	0.6863	0.3880
5 - CFD Vane 2: -15 deg - t=12mm	0.1879	0.0225	0.6892	0.3854
6 - Duct 1.25	0.2069	0.0245	0.6856	0.4540
7 - Duct 2.00	0.2730	0.0327	0.4247	0.7397
8 - Duct 1.30	0.2063	0.0245	0.6919	0.4588
9 - WED	0.2032	0.0241	0.6501	0.4404

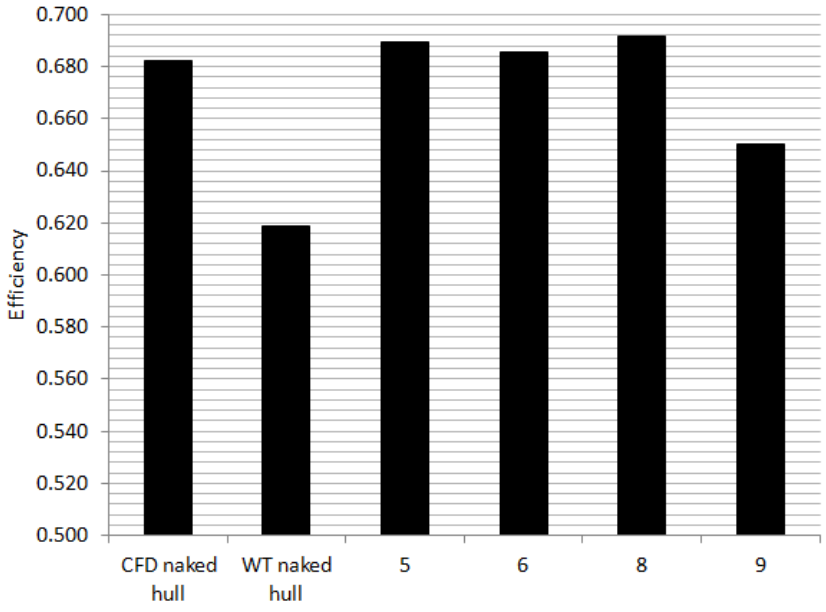

Figure 35: Selection of practical devices

6.3 Discussion

Qualitative data were extracted from CFD to obtain an initial idea of the impact of adding a device on the flow. Figures 32-34 show contour plots of the axial velocity, where each shade represents a variation of $1m/s$. In order to complement the analysis of the flow

field, velocity vector plots are also shown adjacent to the contour plots. Table 7 shows a comparison of all the devices tested in CFD in preparation of the wind tunnel test 2. The propeller parameters K_T, K_Q and η were obtained from the BEMT code. Moreover, the nominal wake was calculated from the local wake matrix derived at the propeller plane.

Vane 1 (1 - 0^o) was first tested to obtain an initial estimate of the influence of a fin on the flow field. The gain in efficiency with Vane 1 was 0.45%. This increase confirms that the initial estimate of the vane location is beneficial to the flow entering the propeller plane. The angle of the vane was then adjusted by 10^o both clockwise and anticlockwise. When angled by $+10^o$, the flow field was directed below the propeller's bottom dead centre, generating vortices. On the other hand, when angled by -10^o, the efficiency increased by 0.77%. This indicated that efficiency gains could be obtained by rotating the vane in the negative direction. Further analyses were performed on a new vane geometry (Vane 2 - longer base). Moreover, the assumed thickness of 20mm was modified to the plywood thickness (12mm) used to build the vanes for the wind tunnel test 2. This last vane was further angled to -15^o and demonstrated an additional gain of 1.03% in efficiency. Indeed, when comparing the velocity plots for the naked hull and with device 5 (Figures 32-33), it may be observed that thanks to the addition of the device, the flow speed increases at top dead centre. As a result, this vane configuration was suggested to be used as an initial set-up for the wind tunnel test 2. However, since the vane was located too close to the bottom wall, bouncing vortices were generated. This phenomenon may have improved the propeller flow field, hence the increase in efficiency. The introduction of a free-surface in CFD would eradicate this unrealistic flow behaviour.

The introduction of a duct (device 6) also showed a gain in efficiency of 0.51%. The initial duct design was modified to an inlet-outlet ratio of 1.3 in order to increase the flow speed into the propeller plane (Figure 34- 'Bernoulli Effect'). This proved an increase of 1.42% in efficiency. The attempt of testing a wake equalising duct in order to create a more uniform flow into the propeller plane was not as successful and it showed a slight decrease in efficiency.

Although the addition of retro-fit devices has shown overall gains in efficiency, the accuracy of the results still needs to be assessed. The differences in efficiency are minimal (below 2%) and may therefore be considered to be within the 'noise'of CFD.

7 TOWING TANK TESTS

In order to increase the physical reality, a free-surface should be added in CFD and the most efficient devices sould then be further tested in a towing tank. An initial test case for the naked hull was set up and verified. The testing of the devices with a free-surface in CFD was left to further work due to time constraint. Towing tank tests were also carried out in both naked and appended hull conditions, but they could be considered to be unreliable due to the innapropritate size of the tank compared to the model used.

7.1 Two-Phase CFD: Inclusion of a Free-Surface

7.1.1 Pre-processing

7.1.1.1 Initial conditions The set up of the towing tank analysis was based around the experiments conducted in the Southampton Solent University towing tank, and a 1:60 scale model. As with the wind tunnel set-up, the geometry was generated using Rhinoceros.

The domain size was matched to the cross section dimensions of the towing tank (3.7m wide $\times$ 1.8m deep) in order to ensure that the same blockage effects were simulated. The height of the liquid fluid phase (fresh water) is equal to the depth of the towing tank. An air phase was required in order to simulate the free surface. The air phase height was defined as 3D (D=depth), allowing enough clearance for the model to be positioned in its desired load condition (ballast). The effect of air resistance on the total resistance is negligible when considering the underwater hull resistance. Therefore, the air phase height does not have a significant impact.

Using the domain analysis conducted on the wind tunnel model, an initial domain length of 1.5L upstream and 2.5L downstream was applied. The boundary conditions applied to the towing tank model were determined to most accurately model the experiments completed. The inlet and outlet boundary field types were defined as a fixed velocity inlet/outlet respectively (U = 1m/s). The hull form was defined as a non-slip wall and all other walls were given a slip condition. The effect of the slip condition was found to have a negligible effect on the flow around the model, when compared to the experimental results.

With all CFD simulations, the computational model is simplified from the complex

physical problem to a practical level. This process induces errors as the computational model is not identical to the experiments. However, the magnitudes of these errors needs to be considered as some can be deemed to be negligible. Indeed, the towing tank experiments were conducted in calm water. Hence, it may be assumed that only sinkage could have an impact on the resistance. As a result, the six degrees of freedom of the towing tank model were eliminated in the CFD simulation. This vastly decreases the simulation complexity as introducing a moving or distorting mesh requires a high level of expertise and takes a considerable amount of time.

7.1.1.2 Mesh generation The mesh generated for the towing tank used the two in-built meshing utilities: blockMesh and snappyHexMesh. Since the wind tunnel results showed a good accuracy, an identical refinement technique was used. Refinement regions were defined along the bilges and at the stern of the tanker hull form. The boundary layer mesh parameters were also taken from the wind tunnel simulations. However, due to the different operating Reynolds numbers, these parameters were modified to generate the desired boundary layer mesh.

The introduction of the free surface caused the largest discrepancy between the wind tunnel and towing tank meshes. Resolving a free surface accurately requires a large number of elements to be concentrated within this region. As a result, a refinement box was positioned along the free surface, using the castellated function, as shown in Figure 36. However, after initial simulations, it was found that further mesh resolution in this region was required since the free surface was not accurately resolved.

To maintain a practical element count, while increasing the refinement on the free surface, a 1D refinement technique was used (Banks 2010). The technique allowed elements to be refined (split) only in the vertical direction. This process can be applied several times although there are limitations. The shape of the elements created was the most important factor. After several refinement iterations, the elements became highly non-orthogonal (flat) and therefore became unsuitable for the simulation. This problem was overcome by using only two refinement iterations. During the first iteration, the cells within $\frac{D}{3}$ on both sides of the free surface are split in half. In the second iteration, only inner cells were further divided (cells within $\pm\frac{D}{6}$) in order to ensure a higher level of accuracy and a smooth growth rate (Figure 38). Furthermore, this process could not be applied to elements adjacent to the boundary layer mesh.

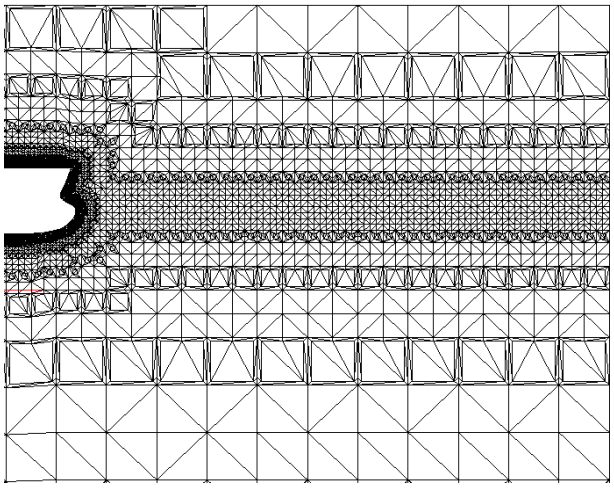

Figure 36: Initial mesh

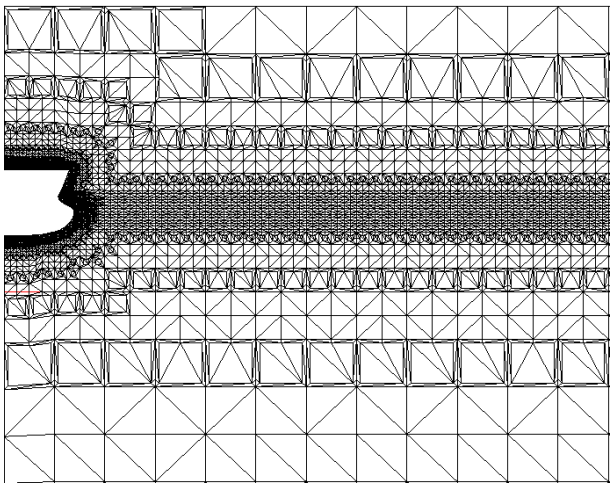

Figure 37: First refinement of free surface

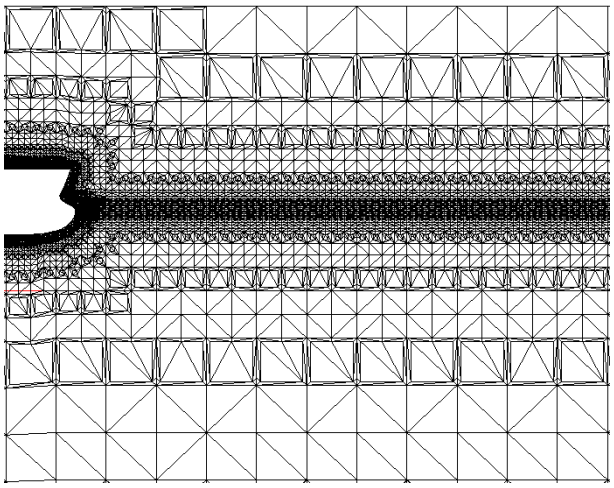

Figure 38: Second refinement of free surface

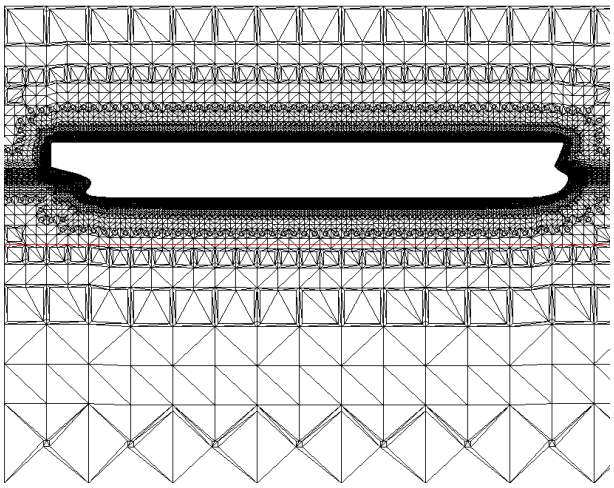

Figure 39: Final mesh

7.1.2 Simulation

Due to the presence of two incompressible isothermal and immiscible fluids (air and fresh water), the interFoam solver was used to resolve the flow properties. This solver is based on a Volume of Fluid (VOF) approach. However, the initial time step used to simulate the flow induced a Courant number greater than 1.0. This problem was solved by reducing the time step which considerably increased the computational time required to study several flow passes around the hull form. In order to solve this problem in a more practical time, the LTS interFoam solver based on a local time stepping was introduced. During the simulation, the time step is modified to obtain a feasible Courant number in regions where the flow becomes highly turbulent (eg. bow wave).

The turbulence model, $k-\omega$ SST, used to solve the flow around the wind tunnel model was also used for the towing tank simulation. The initial parameters k and ω were derived based on an assumed intensity, I, of 5% (for external flow).

The turbulent kinetic energy, k and the dissipation rate, ω, may be expressed as:

$$k = \frac{3}{2}(UI)^2 = \frac{3}{2}(1 * 0.05)^2 = 3.75 * 10^{-3} \qquad [TKE/unit\ mass] \tag{7.1}$$

$$\omega = \frac{k^{\frac{1}{2}}}{l} = \frac{(3.75 * 10^{-3})^{\frac{1}{2}}}{0.01} = 6.12 \qquad [TE/unit\ mass] \tag{7.2}$$

where l is the eddy size, assumed to be 1 cm as for standard external flows.

7.1.3 Results and Analysis

In order to validate the initial set-up for the CFD simulation involving a free-surface, the resistance of the tanker hull form was compared with the experimental data.

Two methods are available in OpenFoam to obtain the forces: 'forcesCoeff'and 'forces'. The drag coefficient may be directly obtained by entering the wetted surface area, fluid density and free stream velocity. Alternatively, each component of the pressure and viscous forces may be extracted in the x-direction, forming the total resistance.

Initially, the forces coefficients were used to evaluate the resistance of the tanker hull form for varying Froude numbers. However, on average, the resistance was overestimated when compared to the towing tank test results, despite having reached a steady-state. The convergence of the drag coefficients is presented in Figure 40 for varying speeds.

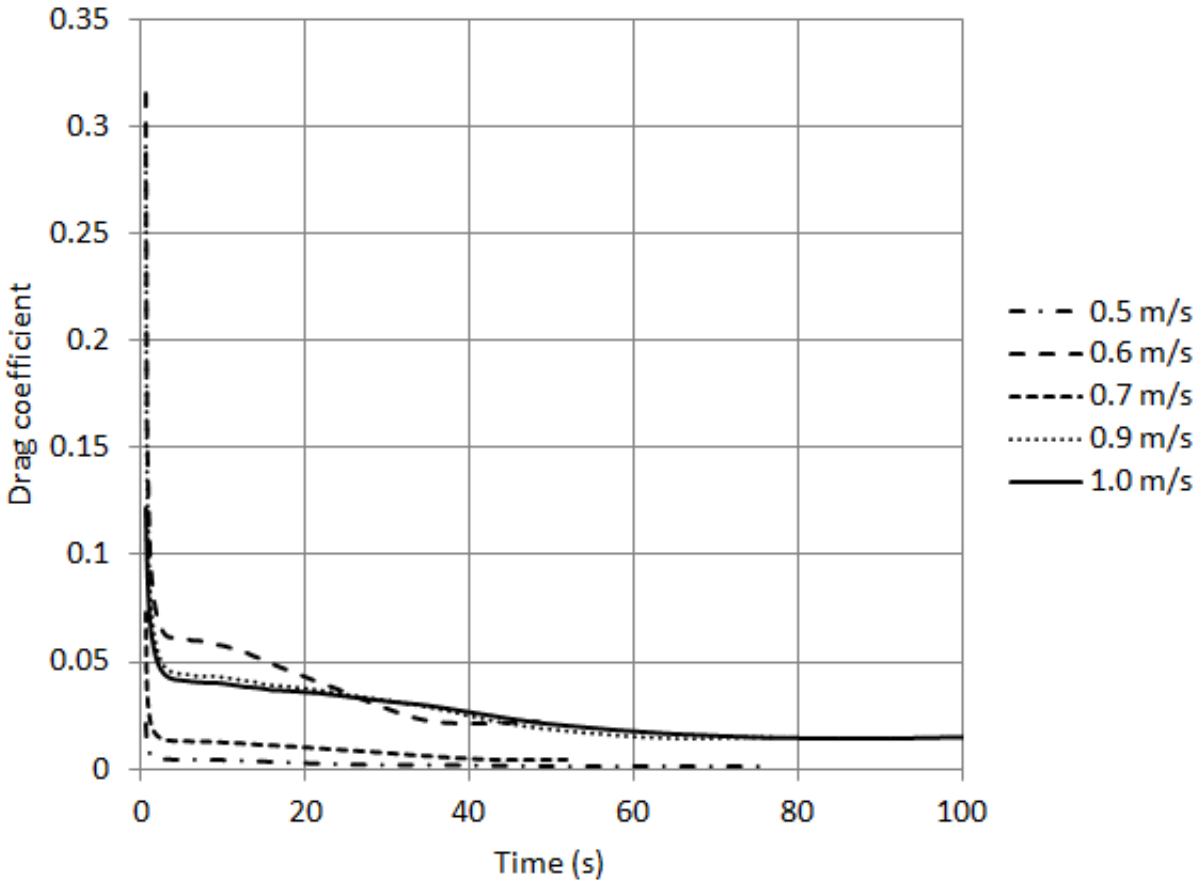

Figure 40: Drag coefficient residuals

The pressure and viscous forces were then analysed separately to determine the source of error. The viscous force was found to be responsible for this discrepancy. To ensure that the forces extracted from OpenFoam were accurate, an alternative technique was used. The wake velocity components were sampled to calculate the viscous resistance based on the Melville-Jones Equation 7.3. This study confirmed the high magnitude of the viscous force as output from OpenFoam.

$$R_V = \rho u^2 \int\int_{wake} (1 - \sqrt{g})(\sqrt{g - p}) dy dz \quad \text{over plane in the wake} \tag{7.3}$$

where $\frac{u_w}{u} = \sqrt{g - p}$ and $g = p + (\frac{u_w}{u})^2$

The magnitude of the viscous force is heavily dependent on the quality of the boundary layer mesh. As a result, an initial mesh dependency study was performed with two other meshes: coarser (1.7 million elements) and refined ($y^+ = 1$ âĂŞ 2.8 million elements). The convergence of the resistance is compared with the initial mesh (medium mesh - 2.3 million elements). As seen in Figure 41, the magnitudes of the resistance are comparable.

Hence, the solution could be considered to be mesh-independent. However, the variation in element count between each mesh is not high enough for a complete mesh dependency study.

This initial investigation was performed to determine both the effects of the free-surface refinement and the boundary layer mesh on the viscous resistance. The coarse mesh was generated with a lower refinement on the free surface. The similarity with the medium mesh confirms that the wave making component of the resistance is appropriately captured. The fine mesh was created with a high boundary layer mesh resolution ($y^+ = 1$). The boundary layer could then be accurately resolved without the need of a wall function ($y^+ = 30$). The viscous resistance obtained with this finer mesh is in agreement with the medium mesh.

Although it was first thought that the forces output from the CFD simulations were too high when compared to the towing tank tests, the above described verification studies may show that the towing tank results should be further assessed. It is suspected that the form factor used was too low.

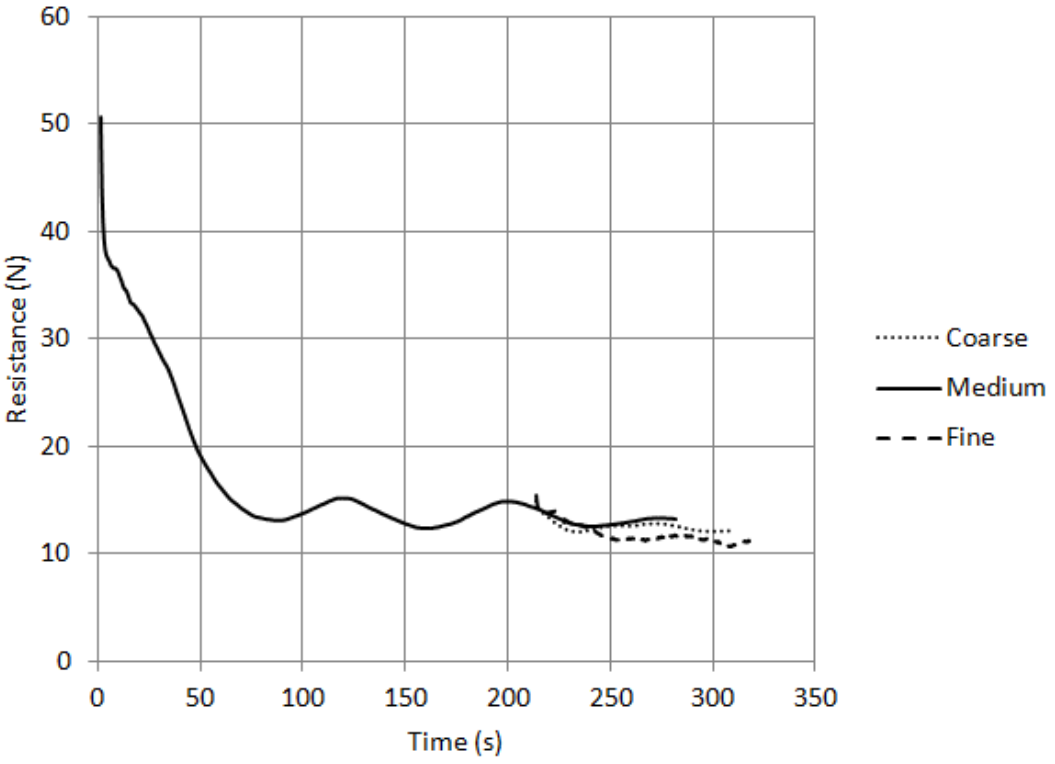

Figure 41: Convergence of resistance for multiple meshes

7.2 Summary of Towing Tests

Further investigations were conducted in the Solent University Towing Tank. A series of naked hull resistance and self-propulsion tests were undertaken using a 1/60 scale geosim ship model. The resistance discrepancy between the naked and appended hull was negligible. Although the normal limits of the towing tank are exceeded (high displacement), definite trends are observed from the variation of device configurations. The decrease in RPM at self-propulsion point after the addition of appendages shows an improvement in performance. The use of the duct, gives a 9.6% gain in the propulsive efficiency. This gain shows the same trend as the results from CFD simulations but these results are suspected to be unrealistically high. In order to obtain more accurate results, a larger scale towing tank would be required and several load conditions should be tested.

8 CONCLUSIONS

Wind tunnel tests are used, in conjunction with open-source computational fluid dynamics modelling, to analyse the wake field changes induced by retro-fit devices. These changes are assessed using the propeller efficiency obtained from blade element momentum theory. A testing procedure is developed, explained in terms of methodology, with justifications for improvements. This procedure successfully detects changes in propeller efficiency at model scale due to devices and thus provides a route to investigate a wide variety of devices.

A cost analysis model was developed to assess the viability of fitting devices on a ship during a routine dry-docking period. Results, based on voyage data provided by the ship operator and European shipyard rates, suggest that a 1% reduction in required delivered power could lead to a payback period of 25 days for devices as simple as a triangular vane. Preliminary results highlight that efficiency gains up to 3% could be obtained with vanes and up to 9% with flow increasing ducts.

9 FURTHER WORK

To validate the current result and further the initial investigations, testing of devices with a greater range of geometries, angles of attack and locations should be carried out. Moreover, the effect of the devices on the wake in several load conditions should be tested. This analysis would provide a clearer understanding of the relationships between the device parameters and the propeller efficiency gains.

Furthermore, a finite element analysis should be used to calculate the structural loading on each device during service. The feasibility of the chosen retro-fit solution could therefore be determined. Such findings would allow further investigations to determine an optimum retro-fit device for the hull form studied.

10 REFERENCES

AZARSINA, F., WILLIAMS, C.D., LYE, L.M. (2006) Resistance and Static Yaw Experiments on the Underwater Vehicle "Phoenix"; Modeling and Analysis, Utilizing Statistical Design of Experiments Methodology. *In OCEANS* Boston MA, 18 - 21 Sept 2006. 1-6.

BANKS, J. (2011) Efficient numerical modelling of the fluid dynamic forces acting on a swimmer, Thesis for transfer from MPhil to PhD, University of Southampton, Fluid structure interactions research group

CARSTENS, R., SIMONSENS, C.D. (2009) Numerical flow simulation of model ship with appendages. Method, validation and investigation of the flow around hull, rudder and propeller, Force Technology, MAN Diesel CFD project report

CONN, J.F.C., FERGUSSON, A.M., (1968) Results Obtained with a Series of Geometrically Similar Models. *Trans. RINA*, 110 (3), 255-300.

CORDIER, S., MORAND, L., ROUX, J-M., CORTEY, E. (2011) Application of OpenFOAMÂő to Hull Form Optimisation at STX France, *RINA Proceedings Marine CFD*

COURANT, R., FRIEDRICHS, K. and LEWY, H. (1967) On the partial difference equations of mathematical physics, *IBM Journal*, 215-234

CRAFT, T., IACOVIDES, H., LAUNDER, B. (unknown) Modelling Felttner Rotors for Ship Propulsion. *Turbulence Mechanics Group*, School of MACE, Manchester University.

DANG, J., CHEN, H., DONG, G., VAN DER PLOEG, A., HALLMANN, R., MAURO, F. (2011) An Exploratory Study on the Working Principles of Energy Saving Devices (ESD's). *Greenship Proceedings 2011*, 96-110.

FLOW SCIENCE (2011) Simulating fluid flows with free surfaces. Available at: http://www.flow3d.com/cfd-101/cfd-101-free-surface-fluid-flow.html (Accessed: 20 November 2011)

FORRESTER, T. J., TINOCO, E., JONG Yu, N. (2005) Thirty years of development and application of CFD at Boeing Commercial Airplanes Seattle, *Computers & Fluids*, 34-10, 1115-1151

GENIZIA, I., PINTO, J., VIANNA, A. (2010) Technological Trends in CFD Applications, *Journal of Technology*, Management & Innovations, 5-2, 76-83, ISSN: 0718-2724

HAFERMANN, D., SCHNEIDER, M., RICHARDS, J.,CHAO, K., TAKAI, M. (2010) Investigation of Propulsion Improving Devices with CFD, *11th International Symposium on Practical Design of Ships and Other Floating Structures*, Rio de Janeiro, Brazil

HANSEN, H.R., DINHAM-PEREN, T., NOJIRI, T. (2011) Model and Full Scale Evaluation of a 'Propeller Boss Cap Fins' Device Fitted to an Aframax Tanker. *Second International Symposium on Marine Propulsors*

HASSEN, G.L., JAMES, R.W. (1960) Optimum ship routing, *Journal of Navigation*, 13(3)

KORNEV, N., TARANOV, A., SHCHUKIN, E., KLEINSORGE, L., (2010) Development of hybrid RANS-LES methods for flow simulations in ship stern area using OpenFOAM, *CFD Workshop*, Gothenburg

IMO (2009) Interim Guidelines on the Method of Calculation of the Energy Efficiency Design Index for New Ships *MEPC.1/Circ 681 Ref. T5/1.01*

IMO (2011) Reduction of GHG Emissions from Ships *MEPC 62/5/17*

ITTC (2011) The resistance committee, *26th International Towing Tank Conference*, Rio de Janeiro

JIJUN, C., CHENGSHENG, W., ZIYING, P., WENTAO, Z. (2011) Evaluation for a Sail-assisted Bulk Carrier Operating on the Route of Hong Kong - Yokohama *Greenship Proceedings 2011*

KIM, W.J., KIM, D.H., VAN, S.H. (2001) Measurement of Flows Around Modern Commercial Ship Models. *Experiments in Fluids* , 31, 567-578

MAKINO, K., MASUDA, S. (2008) Simulation of the Flow Field around the Ship with Energy Saving Device by Using CFD, *The Japan Society of Naval Architects and Ocean Engineers*, 6, 135-138

MARIA, V.G., LUNGU, A. (2011) Numerical study of the wake field produced by a hull retrofitted with flow control devices, *AIP conference proceedings*, 203-206

MC NEEL (2010) What is NURBS?. Available at: http://www.rhino3d.com/nurbs.htm (Accessed: 16 October 2011)

MENTER, F. R. (1993) Zonal Two Equation k-ÏĽ Turbulence Models for Aerodynamic Flows, *AIAA Paper*, 93-2906

MEWIS, F., GUIARD, T. (2011) Mewis Duct - New Developments, Solutions and Conclusions *Second International Symposium on Marine Propulsors*

MOIN, P., MAHESH, K. (1998) Direct numerical simulation: a tool in turbulence

research, *Fluid Mechanics*, 30, 539-578

MOLLAND, A.F., TURNOCK S.R., HUDSON D.A. (2011) *Ship Resistance and Propulsion. Practical Estimation of Ship Propulsive Power* New York: Cambridge University Press

MOLLAND, A.F., TURNOCK S.R.,(2007) *Marine Rudders and Control Surfaces; Principles, Data, Design and Applications* Oxford: Elsevier

NAFEMS (2010) Guidelines for Good Convergence in CFD. Available at: http://nafems.org/resources/cfdconvergence/Page0/ (Accessed: 2 February 2011)

NAKASHIMA, T., DOI, Y., MUTSUDA, H., SATAKE, S., OGAWA, T. (2009) Numerical analysis on wind drag reduction of accommodation house with square corner cut and step shaped geometry, *Journal of Japan Society of Naval Architects and Ocean Engineers*, 9, 87-95

ORIHARA, H., MIYATA, H. (2003), Evaluation of added resistance in regular incident waves by computational fluid dynamics motion simulation using an overlapping grid system, *Journal of Marine Science and Technology*, 8 (2), 47-60

PATEL, V.C., SARDA, O.P. (1990) Mean-Flow and Turbulence in the Boundary Layer and Wake of a Ship Double Model. *Experiments in Fluids*, 8 (6), 319-335

RICHARDSON, L.F. (1910) On the approximate arithmetical solution by finite differences of physical problems involving differential equations with an application to the stresses in a masonry dam, *Royal Society London Proceedings*, 83

SCHLICHTING, H., GERSTEN, K. (2000) *Boundary-layer Theory*, Springer 8th edn., ISBN 3540662707

SOUTO-IGLESIAS, A., ZAMORA-RODRIGUEZ, R., FERNANDEZ-GUTIERREX, D., PEREZ-ROJAS L. (2006) Analysis of the wave system of a catamaran for CFD validation, *Experiments in fluids*, 42(2), 321-332

WILCOX, D.C. (2006) *Turbulence Modelling for CFD*, 3rd edn., California: Birmingham Press

XING, T., CARRICA, P., STERN, F. (2008) Computational towing tank procedures for single run curves of resistance and propulsion, *Journal of Fluids Engineering*, 130 (6)

ZONDERVAN, G-J., HOLTROP, J., WINDT, J., TERWISGA, . (2011) On the Design ans Analysis of Pre-swirl Stators for Single and Twin Screw Ships. *Second International Symposium on Marine Propulsors*